Heterogeneous and Aging Dynamics in Single and Stacked Thin Polymer Films

Koji Fukao*, Takehide Terasawa, Kenji Nakamura, and Daisuke Tahara

Abstract The glass transition and the α-process above the glass transition temperature, T_g, and the aging dynamics below T_g were investigated for single and stacked thin polymer films. First, the glass transition dynamics of stacked thin films of polystyrene (PS) and poly(2-chlorostyrene) (P2CS) were measured using differential scanning calorimetry and dielectric relaxation spectroscopy. The T_g for as-stacked thin PS films has a strong depression from that of the bulk samples. However, after annealing at high temperatures above T_g, the stacked thin films exhibit glass transition at a temperature almost equal to the T_g of the bulk system. The α-process dynamics of stacked thin films of P2CS show a very slow time evolution from single thin film-like dynamics to bulk-like dynamics during the isothermal annealing process. The temperature dependence of the relaxation time for the α-process changes from Arrhenius-like to Vogel-Fulcher-Tammann dependence with increase of the annealing time. Secondly, the aging dynamics of P2CS ultrathin films with thicknesses less than 10 nm were investigated using dielectric relaxation spectroscopy. The imaginary part of the dielectric susceptibility, ε'', for P2CS ultrathin films with a thickness of 3.7 nm increases with an increase in isothermal aging time, while this is not the case for P2CS thin films thicker than 9.0 nm. This anomalous increase in ε'' for the ultrathin films is strongly correlated with the presence of a mobile liquid-like layer within the thin films.

Keywords

Heterogeneous dynamics · Aging dynamics · Stacked thin polymer films · Glass transition · Interfacial interaction · Memory and rejuvenation effects

K. Fukao (Corresponding author), T. Terasawa, K. Nakamura, D. Tahara
Department of Physics, Ritsumeikan University, Noji-Higashi 1-1-1, Kusatsu, 525-8577 Japan
e-mail: fukao.koji@gmail.com

Contents

1 Introduction

If a material in the liquid state at high temperature is cooled down in an appropriate manner, the material can often keep the liquid state even below the melting temperature, which is called supercooled liquid state. Then, further cooling of the supercooled liquid enables us to obtain a solid state with disordered molecular arrangement similar to the liquid state but without any mobility characteristic of the liquid state, if no crystallization occurs during the further cooling [1]. This disordered solid state is the glassy state and the transition from the liquid state to the glassy state via the supercooled liquid state is known as the glass transition and the temperature at which the glass transition occurs defines the glass transition temperature T_g. It should be noted that the glassy state is a non-equilibrium state. The

understanding of the mechanism of the glass transition remains one of the most important unsolved problems in the condensed matter physics [2], although there have been many approaches not only from experimental and theoretical viewpoints but also from simulational ones [3].

The results observed so far have revealed several anomalous dynamical behavior related to the glass transitions. First, the characteristic time τ_α of the main motion excited in the liquid states, which is the α-process, becomes extraordinarily longer with decreasing temperature down to T_g in a manner given by

$$\tau_\alpha^{-1} = \tau_{\alpha,0}^{-1} \exp\left(-\frac{U}{T-T_0}\right), \tag{1}$$

where $\tau_{\alpha,0}$ is a characteristic time of an elementary process of the α-process, U is an apparent activation energy and T_0 is the Vogel temperature, which is by about 50 K lower than T_g. This is called the Vogel-Fulcher-Tammann (VFT) law [4]. Hence, it is expected that the time scale of the α-process becomes a macroscopic time scale, *i.e.*, 10^2-10^3 sec at T_g. As a result, the molecular mobility induced by the α-process is almost lost and the disordered structure is totally frozen in the glassy state. Secondly, the relaxation function $\phi(t)$, which is obtained by several relaxation measurements such as dielectric relaxation spectroscopy, viscoelastic measurements and so on, is given not by the single exponential function but by the stretched exponential function :

$$\phi(t) = \exp\left[-\left(\frac{t}{\tau_K}\right)^{\beta_K}\right], \tag{2}$$

where β_K is the stretching parameter and $0 < \beta_K < 1$ and τ_K is a relaxation time ($\tau_K \approx \tau_\alpha$ for the α-process) [5]. The observed relation that $0 < \beta_K < 1$ means that there are distributions of the relaxation times τ_α of the α-process in real systems, in other words, there are many motional units with different characteristic times. Recent further investigations clearly show that the motional units of the α-process with various values of τ_α move not independently but in a collective manner. This type of character of the molecular motion is usually known as *dynamical heterogeneity* [6, 7]. Within the system, there are several domains with slower motions or faster motions. As temperature approaches from high temperature to T_g, the dynamical heterogeneity grows significantly especially in the supercooled liquid state, and hence this can be believed as one of the most important characters of dynamical nature of the glass transition. According to this scenario, there should be a length scale which characterizes the dynamical heterogeneity in the liquid states near the glass transition. This idea is associated with a cooperative rearranging region (CRR) which has been proposed by Adam and Gibbs long time ago [8]. Therefore, the experimental approaches to such characteristic length scale of the glass transition and the α-process have been important issues which should be clarified in order to elucidate the mechanism of the glass transition.

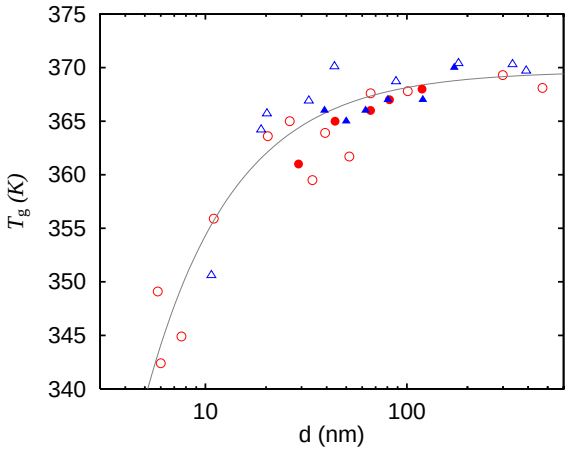

Fig. 1 Thickness dependence of the glass transition temperature of atactic PS films obtained during the heating process (○ corresponds to M_w=2.8×10^5, and △ to M_w=1.8×10^6). The values of T_g are determined as the crossover temperature between the straight lines characterizing the real part of electric capacitance $C'(T)$ at 10kHz below and above T_g. The symbols ● and ▲ represent the data obtained for uncapped supported films of atactic PS by Forrest *et al.* using ellipsometry for atactic PS (M_w=7.67×10^5 (●), 2.2×10^6 (▲)) [9]. The solid curve was obtained from the layer model [21].

1.1 Glass transition of thin polymer films

If there is a characteristic length scale of the glass transition and the α-process, it can be expected that there is an appreciable change of the glass transition dynamics as the system size decreases down to the length scale. From such motivation, many investigations on the glass transition in small scales or confined systems, namely, the glass transitions of small molecules in nanopores or thin polymer films, have widely been performed since 1990s [10]. The investigations on confined systems have revealed that the T_g of thin polymer films or small molecules in a confined geometry decreases with decreasing film thickness or size of nanopores in many cases if there is no strong attractive interaction of polymers or small molecules with surrounding material, although there are some contradictory results [11–30]. As a typical example, Fig. 1 shows the glass transition temperature of thin films of polystyrene (PS) supported on substrate measured by dielectric measurements and elipsometric measurements. In this figure T_g of thin PS films decreases with decreasing film thickness regardless of the method of measurements. For physical origins for the depression of the T_g there are several candidates such as surface or interfacial effects [31], confinement effects in thin film geometry [10], and so on. The physical origin has not yet been determined but is still in debate.

In addition to the glass transition of the single thin films, we here refer to the glass transition of stacked thin polymer films, where the stacked films consist of many ultrathin polymer layers, for example, thin layers with thickness of about 10 nm and the total thickness is μm-scale order, that is, the thickness of bulk films. For

such stacked thin films, we have a question whether the glass transition behavior for the stacked thin polymer films has thin-film like properties or bulk-like ones. In the literature an answer to this question can be found. The glass transitions of stacked thin films have been investigated using differential scanning calorimetry (DSC) by Simon *et. al.* [32, 33]. The glass transition temperature T_g of stacked thin PS films is dependent on the thickness of the single layers of the stacked thin films, which is similar to that for single thin polymer films. Furthermore, T_g is increased by annealing above T_g and approaches that of the bulk system, which suggests that stacked thin films prepared by an appropriate method can maintain the thin-film properties of the glass transition dynamics. This result suggests that the existence of the interface between thin polymer layers can decrease the T_g, and hence the interfacial interaction can control the depression of T_g.

1.2 Aging phenomena of polymer glasses

As mentioned in the above, the molecular mobility due to the α-process is almost lost in the glassy state [1], because the characteristic time of the α-process becomes macroscopic time scale below T_g. In polymeric systems, segmental motion is the microscopic origin of the α-process [34] and this motion is almost frozen in the glassy states. However, even in the glassy state there is a very slow change in the structure and dynamics when approaching an equilibrium state, and this phenomenon is known as physical aging [35]. Several interesting phenomena, including *memory and rejuvenation effects*, occur during physical aging [35–37]. These effects are frequently observed in many disordered systems, including polymer glasses [38–43], spin glasses [44–47], and other disordered systems [48–50].

We have previously investigated the aging dynamics in polymer glasses of poly(methyl methacrylate) (PMMA) [40–42], PS [51,52], and poly(2-chlorostyrene) (P2CS) [53] using dielectric relaxation spectroscopy and temperature modulated differential scanning calorimetry. In PMMA, the real and imaginary parts of dielectric susceptibility, ε' and ε'', decrease with increasing aging time for isothermal aging. This result is consistent with the idea that the non-equilibrium glassy state approaches an equilibrium state. An example of the memory and rejuvenation effects of the dielectric susceptibility for the aging dynamics observed in PMMA are shown in Fig. 2.

In Fig. 2, the time evolution of dielectric susceptibility has been measured for the thermal history which consists of the series of the three isothermal annealing processes at the temperatures T_1, T_2, and T_1 for time τ_1, τ_2, and τ_3, respectively. This thermal history is called temperature cycling mode (TC mode). Here, the value of T_2 is set to be lower than the one of T_1. Figure 2 shows time dependence of $\varepsilon'' - \varepsilon''_{\rm ref}$ for PMMA thin films with the thickness d=26 nm, T_1=374.2K, T_2=354.6K, and $\Delta T \equiv T_1 - T_2$=−19.6K. The origin of the time (t_w=0) is defined as the time when the temperature reaches T_1 after cooling from 403 K (above T_g). The value of $\varepsilon''_{\rm ref}$ is the reference value of ε'' for each aging temperature (T_1 or T_2). In this

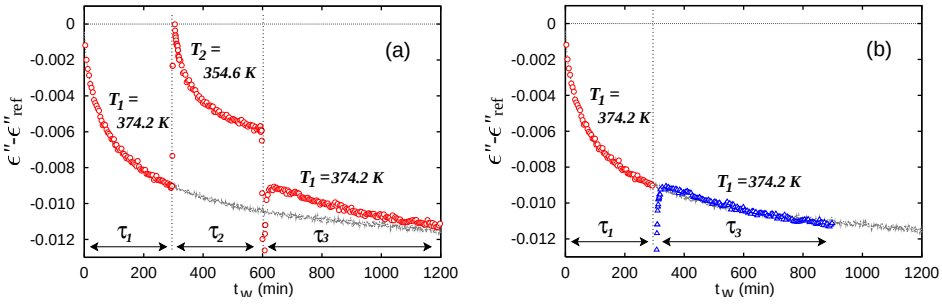

Fig. 2 (a) Aging time dependence of the difference between ε'' and $\varepsilon''_{\rm ref}$ observed by the TC mode with T_1=374.2 K and T_2=354.6 K (ΔT=−19.6 K) for PMMA thin films with d=26 nm. (b) The difference $\varepsilon'' - \varepsilon''_{\rm ref}$ obtained by shifting the date points in the third stage in the negative direction of the time axis by τ_2 after removing the data points in the second stage. Aging times at the first and second stages are $\tau_1 = \tau_2 = 5$ hours. The horizontal axis of Fig. 2(b) is the total aging time at T_1. The solid curve is the standard relaxation one obtained by isothermal aging at 374.2 K.

case, the value of $\varepsilon''_{\rm ref}$ for T_1 (T_2) is the initial value of ε'' obtained at the time when the temperature reaches T_1 (T_2) directly from 403 K. As the aging time t_w increases from 0, $\varepsilon'' - \varepsilon''_{\rm ref}$ decreases. This decrease in ε'' corresponds to *aging*. At $t_w = \tau_1$, the temperature is lowered from T_1 to T_2, and then $\varepsilon'' - \varepsilon''_{\rm ref}$ immediately changes to 0. This indicates that the decrease in temperature from T_1 to T_2 causes the polymer sample to *rejuvenate*. As the aging time elapses at T_2, $\varepsilon'' - \varepsilon''_{\rm ref}$ relaxes from 0 just like a new relaxation process starts at $t = \tau_1$. At $t_w = \tau_1 + \tau_2$, the system is heated up to T_1, and then the temperature of the system is kept at T_1. On this stage, $\varepsilon'' - \varepsilon''_{\rm ref}$ goes back to the value which $\varepsilon'' - \varepsilon''_{\rm ref}$ had reached at $t_w = \tau_1$ and then begins to decrease as if there were no temperature change during the aging process at T_1.

In Fig. 2(b) is shown the time evolution of $\varepsilon'' - \varepsilon''_{\rm ref}$ after removing the data between τ_1 and $\tau_1 + \tau_2$ and shifting the data for $t_w > \tau_1 + \tau_2$ in the negative direction along the time axis by τ_2. In this figure, we can see that $\varepsilon'' - \varepsilon''_{\rm ref}$ decreases monotonically with the aging time without any discontinuous change except for a short region just after τ_1. The curve obtained in the above way agrees very well with the curve obtained by keeping the system at T_1 without any temperature change. This implies that polymer glasses can remember the state at $t_w = \tau_1$ of the relaxation towards the equilibrium state and recall the memory at $t_w = \tau_1 + \tau_2$. In this case, we can say that there is a *memory effect*.

The memory and rejuvenation effects can also be observed for another thermal protocol, *i.e.*, constant rate mode (CR mode). In this CR mode, two serial ramping processes between 273 K and 403 K are done. The first one consists of cooling and heating processes at the rate of 0.5 K/min and this is defined as the reference process. The second one is the same to the first one except the addition of an isothermal aging process at a given temperature T_a (T_a is located below T_g of PMMA). The difference of the dielectric susceptibility between the first and second ramping process, $\varepsilon' - \varepsilon'_{\rm ref}$, is obtained as the effective contributions of isothermal aging to ε'. Figure 3 displays the temperature change in $\varepsilon' - \varepsilon'_{\rm ref}$ obtained by the CR mode with various

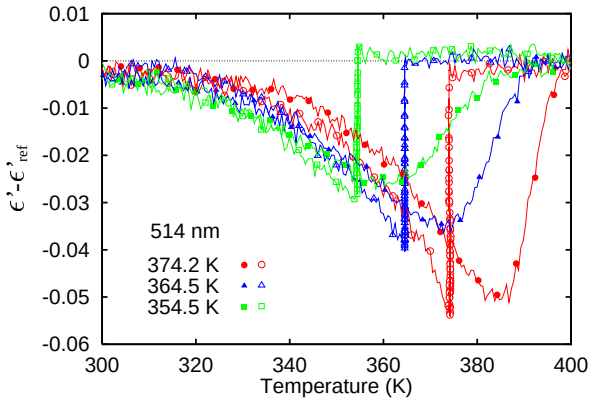

Fig. 3 Temperature dependence of the difference between ε' and $\varepsilon'_{\rm ref}$ observed by CR mode with three different aging temperatures T_a=374.2 K, 364.5 K and 354.5 K for PMMA films with d=514nm. The frequency of the applied electric field f is 20Hz. The heating and cooling rates were 0.5 K/min and the aging times at T_a was 10 hours. Open and full symbols display the data observed during the cooling and heating processes, respectively.

aging temperatures T_a for $d = 514$ nm. In Fig. 3, it is found that, as the sample is cooled down from 403 K to T_a, ε' is almost equal to $\varepsilon'_{\rm ref}$ and the difference $\varepsilon' - \varepsilon'_{\rm ref}$ remains zero. The difference then begins to deviate from 0 to a negative value and the deviation becomes larger monotonically with increasing aging time during the subsequent isothermal aging at T_a. This indicates that ε' decreases with aging time at T_a. As the temperature decreases from T_a to room temperature after the isothermal aging, the difference $\varepsilon' - \varepsilon'_{\rm ref}$ decreases with decreasing temperature and becomes almost zero at room temperature. Just after the temperature reaches 293 K, the heating process begins. As the temperature increases, the difference $\varepsilon' - \varepsilon'_{\rm ref}$ begins to deviate from 0 to a negative value almost along the same way as observed during the preceding cooling process. The difference between ε' and $\varepsilon'_{\rm ref}$ exhibits a maximum at around T_a+10K and then decreases to 0 with increasing temperature.

This behavior observed by the CR mode can be interpreted as follows: the thermal history that the sample is aged at T_a for 10 hours is *memorized* at T_a during the cooling process. As the temperature decreases from T_a to room temperature, the sample begins to *rejuvenate* and is back to almost a standard age at room temperature. During the subsequent heating process, the sample becomes older almost according to the curve along which the sample experienced rejuvenation during the preceding cooling process after a temporary stop at T_a. This result implies that not only the aging process at T_a near T_g but also the subsequent cooling process can be memorized and the whole thermal history can be read out during the heating process.

The above two temperature protocols clearly show the existence of interesting memory and rejuvenation effects. As shown in Sec. 1.1, recent researches have shown that segmental motion, which is frozen in the glassy state, is strongly dependent on the film thickness [11, 20]. The value of T_g decreases with decreasing

film thickness, and accordingly, the dynamics of the α-process, the segmental motion, become faster in thinner films [20, 21, 54, 55]. Therefore, it is very natural to expect that there should be a characteristic thickness dependence of the aging dynamics in thin polymer films. There have been several reports on the dependence of the aging dynamics on thickness [40, 56–59].

1.3 Heterogeneous and aging dynamics in single and stacked thin polymer films

As mentioned in Sec. 1.1 and 1.2, we developed our researches on the glass transition of polymeric systems in two different ways. First, we investigated dielectric relaxation behavior of thin polymer films in order to elucidate how the glass transition dynamics change over the range from the liquid state to the supercooled liquid state near T_g when the system size changes from bulk to *nm* scale in thin film geometry. Through this series of investigations, we could show the significant contributions of the surface and interfacial dynamics to the glass transition dynamics, and now we have moved to the investigation on the glass transition of stacked thin polymer films [60, 61]. Secondly, we investigated the aging dynamics of polymer glass below T_g and showed the existence of the common aging phenomena both for polymer glass and spin glass, and then we have continued the investigation on the nature of the memory and rejuvenation effects observed for aging process and how the confinement in thin film geometry affects on the aging dynamics [53, 62]. We believe that such investigations on the glass transition dynamics both from the liquid state to T_g and from the glassy state to T_g are quite important. The true understanding of the basic mechanism of the glass transition might not be obtained before the researches from both the directions could be connected with each other.

Here, we would like to show our recent results on the glass transition dynamics of stacked thin polymer films and the aging dynamics of ultrathin polymer films investigated by differential scanning calorimetry and dielectric relaxation spectroscopy. For both cases, heterogeneous dynamics such as the surface and interfacial dynamics play a crucial role for determining the characteristic features. Through the two different researches related to the heterogeneous dynamics, it can be expected that a clearer view of the glass transition could be obtained.

In this article, we show the experimental results on the glass transition and aging dynamics for single and stacked thin films of PS and P2CS, observed along the two different directions as shown in this above. After giving the experimental details in Sec. 2, the glass transition temperatures are given as a function of thickness for single thin films of P2CS in Sec. 3. Then, the glass transition dynamics of stacked thin films of P2CS are discussed in Sec. 4 and the aging dynamics of the ultrathin P2CS films are done in Sec. 5. Finally, a summary is given in Sec. 6.

2 Experiments

2.1 Sample preparation

P2CS and PS used in this study were purchased from Polymer Source, Inc, and General Science, Co. Ltd., respectively. The weight-averaged molecular weight, M_w, and the molecular weight distribution (M_w/M_n, where M_n is the number-averaged molecular weight) were $M_w = 3.3\times10^5$ and $M_w/M_n = 2.2$ for P2CS, and $M_w=2.8\times10^5$ for PS. The structure of P2CS is similar to that of PS, except for the presence of a chlorine atom on the benzene ring. However, the polarity of P2CS is much larger than that of PS; therefore, P2CS can be regarded as an ideal system for the dielectric measurements.

Using spin-coating, we prepared single thin films of P2CS for dielectric measurements from a toluene solution on a glass substrate on which aluminum (Al) had been vacuum deposited. The film thickness was controlled by varying the concentration of the solution. After annealing at 343 K under vacuum for two days to remove solvents, Al was again vacuum deposited to serve as an upper electrode. The thickness was evaluated before measurements from the value of the electrical capacitance at 273 K for the as-prepared films in the manner previously reported [20, 21]. The absolute thickness is also obtained by direct measurement using atomic force microscope.

Stacked thin films were prepared in the following way [60]. Single ultrathin films of various thickness were prepared on glass substrates by spin coating of a toluene solution, as shown in the above. The film was floated onto the surface of water and transferred to the top of a substrate or a stack of polymer thin films on a substrate. This procedure, using ultrathin films with the same thickness, was repeated until the total number of stacked thin layers reached several hundred for the DSC measurements and 10 layers for the dielectric measurements, as listed in Tables 1 and 2. For the dielectric measurements, the first layer of P2CS was prepared directly onto an Al-deposited glass substrate and subsequent thin layers were prepared according to the above procedure. For the DSC measurements, a Teflon plate was used as a substrate. The stack of thin films, which consisted of several hundred thin layers, were detached from the Teflon substrate using a razor blade.

Table 1 Thickness of a single layer d, total weight, number of stacked layers, and T_g (K) measured by DSC for stacked PS thin films prepared for the DSC measurements.

d (nm)	weight (mg)	No of layers	T_g (K)
70	0.623	73	369
55	0.528	100	364
40	0.611	130	361
20	0.786	224	353
13	0.899	400	350
Bulk	1.361	1	376

Table 2 Thickness of a single layer d, number of stacked layers, isothermal annealing temperature T_A, and T_g (single thin film with a thickness of d) for stacked P2CS thin films prepared for the dielectric relaxation measurements. *The value of T_g is evaluated for a single thin film with thickness d, rather than the total stack thickness, from an approximation given by Eq.(3) in this article.

d (nm)	No. of layers	T_A (K)	T_g (K)*
18.5	10	425	381.0
15.4	10	416	380.1
10.0	10	412	378.6
9.6	10	422	378.5

2.2 Measurements for stacked thin polymer films

DSC measurements were performed in order to determine the T_g of the stacked PS thin films as listed in Table 1. A commercial instrument (TA Instruments, Q200) was used for the measurements. The DSC run was firstly conducted for the heating process from 303 to 403 K at a rate of 10 K/min, and then for the cooling process down to 303 K at the same rate. The measurements were repeated three times to confirm reproducibility. The stacked samples used for the DSC measurements were then annealed at 523 K for 12 h in vacuo. Nitrogen gas was flowed at 30 mL/min during the DSC measurements.

Dielectric measurements were performed in order to investigate the dynamics of the α-process of the stacked P2CS thin films as listed in Table 2. An LCR meter (Agilent Technology, 4284A) was used for the dielectric measurements. One measurement for the frequency f range from 20 Hz to 1 MHz took approximately 50 s. Prior to the dielectric measurements, several heating and cooling processes through T_g were conducted for stabilization of the measurements. Following that, the dielectric measurements were performed repeatedly for the following temperature cycles. One temperature cycle consists of two successive parts:
(1) Cooling and heating processes between 433 and 273 K at a rate of 1 K/min were conducted *twice*.
(2) After the ramping process, the temperature was changed from 433 K to T_A (= 412$\sim$425 K) and was then kept at T_A for 10 h (isothermal annealing at T_A).

These measurements showed that the two dielectric loss spectra observed successively in the temperature domain at a given frequency in part (1) agree with each other; therefore, the annealing effect for the ramping process (1) between 273 K and 433 K was determined to be negligible compared with that for the isothermal annealing process. The annealing time t_a can be well-defined by the total time for which the films remain at the annealing temperature T_A. Hence, t_a for the n-th isothermal annealing cycle starts from $10\times(n-1)$ h.

2.3 Measurements of aging dynamics in thin polymer films

Dielectric measurements were carried out in the same experimental setup described in Sec. 2.2 for the ultrathin films of P2CS with thickness d of 3.7, 5.4, 9.0, 9.5, and 22 nm, in order to investigate the aging dynamics below T_g. The complex dielectric constant $\varepsilon^*(\equiv \varepsilon' - i\varepsilon'')$ was evaluated as a function of temperature T, aging time t_w, and the frequency of applied electric field f. The value of ε^* was obtained from the value of the complex electrical capacitance of the sample condenser $C^*(\equiv C' - iC'')$, on the assumption that C^*=$\varepsilon^* C_0$ is valid, where C_0 is the geometrical capacitance of the sample condenser.

For the investigation of the aging dynamics, the following two temperature protocols were employed:

1) *Isothermal aging*: In this temperature protocol, the temperature was changed from a high temperature of 425 K (above T_g) to an aging temperature T_a (below T_g), and then the temperature was maintained at T_a for t_a hours.

2) *Constant-rate mode*: The temperature was decreased from 425 to 273 K at a constant rate of 1 K/min, and then increased from 273 to 425 K at the same rate. This is a simple constant-rate mode and we refer to this temperature change as the reference mode. In addition to the above thermal treatment, we included an intermittent stop at T_a for t_a hours during cooling from 425 to 273 K. This temperature protocol is denoted as $\mathscr{C}(T_a, t_a)$. According to this notation, the reference mode corresponds to the protocol $\mathscr{C}(T_a, 0)$ for any value of T_a.

3 Glass transition temperature of thin P2CS films

Before showing the results of glass transitions dynamics of stacked thin films and aging dynamics of the ultrathin P2CS films, the thickness dependence of T_g of single thin films of P2CS supported on the Al-deposited glass substrate is shown in Fig. 4. The value of T_g was determined from the measurements of the electric capacitance (dielectric constant) for the ramping process with a constant rate, in this case, at the rate of 1 K/min. As shown in Ref. [20, 21], the temperature coefficient of the real part of electric capacitance C' observed for high frequency (i.e., 100 kHz) changes significantly through the glass transition temperature, because the thermal expansion coefficient of the glassy state is much smaller than that of the liquid state. On the basis of this property, T_g can be determined from the crossover temperature of C' observed during the ramping process at a constant rate. Fig. 4 clearly shows that T_g of single thin P2CS films decreases with decreasing film thickness in a similar way observed for thin films of PS. The observed thickness dependence is given as follows [60]:

$$T_g(d) = \begin{cases} \Delta T_g(d - d_c) + T_{g,c} & : \quad d < d_c \\ T_{g,\infty} - \dfrac{d_c}{d}(T_{g,\infty} - T_{g,c}) & : \quad d > d_c, \end{cases} \tag{3}$$

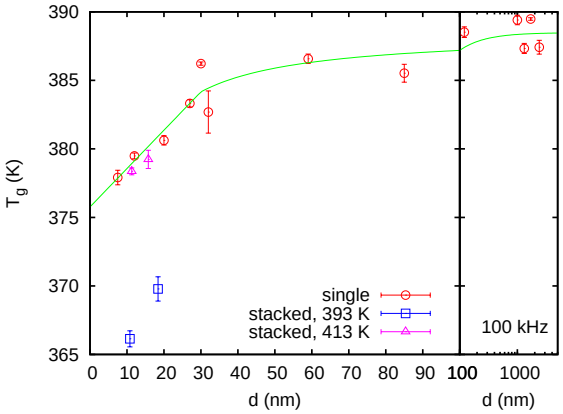

Fig. 4 Thickness dependence of T_g for thin films of P2CS determined as a crossover temperature in the electric capacitance. ○ stands for T_g of the single thin films and □, △ are T_g of the stacked thin films annealed at 393 K and 413 K, respectively. In the latter case, the thickness of the horizontal axis is the averaged thickness of each single layer within 10 stacked thin films.

where ΔT_g=0.28±0.07 K/nm, d_c=30±11 nm, $T_{g,c}$= 384.2±2.7 K, $T_{g,\infty}$=388.5±0.6 K. The thickness of the as-prepared films was evaluated from electrical capacitance measured at 273 K, according to a previously reported procedure [20,21]. It should be noted that the value of T_g for bulk films is about 18 K higher for P2CS than for PS.

4 Glass transition dynamics of stacked thin polymer films

A similar measurement of T_g has been performed for not only single thin films but also stacked thin films of P2CS [60]. The observed T_g for stacked thin films has been plotted in Fig. 4, also. In this figure, it is found that T_g for stacked thin films of P2CS annealed at 393 K for 2 hours (See the symbol □) is located far below the bulk T_g and furthermore about 10 K below the T_g of the single thin film with the same thickness (See the symbol ○). This result suggests that the stacked thin films can keep the T_g of the single thin films even after stacking 10 thin layers. In the case of PS thin films, it has been reported that the magnitude of the depression of T_g of the freely standing films is by about 50 K larger than that of the supported thin films [9, 65]. If the magnitude of the depression of T_g of the freely-standing thin films of P2CS can obey the same law for PS, it is concluded that the T_g of the stacked thin films of P2CS is located between the supported single thin films and the freely standing films. This result is consistent with the results observed for PS stacked thin films [33]. In Fig. 4, the value of T_g of stacked P2CS thin films annealed at 413 K for 2 hours is larger than the one annealed at 393 K and almost equal to the value of the single P2CS thin films with the corresponding thickness.

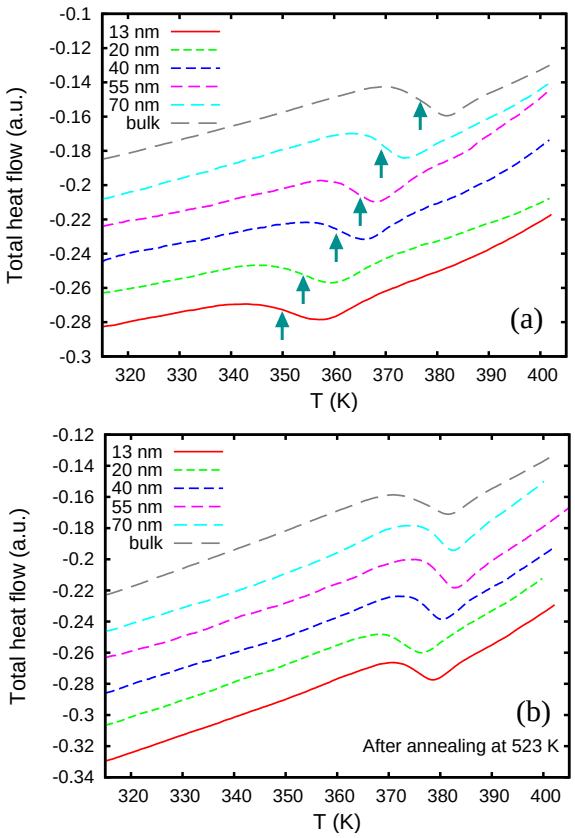

Fig. 5 Temperature dependence of the total heat flow for stacked PS thin films with various single layer thicknesses, from 13 nm to that of the bulk value, during the heating process at a rate of 10 K/min. (a) As-stacked thin PS films, and (b) after annealing at 523 K for 12 h. Each curve is shifted slightly along the vertical axis for ease of comparison.

The above results can be summarized as follows: 1) the T_g of single P2CS thin films was found to decrease with decreasing film thickness in a similar way to that observed for PS thin films [11, 20, 21]. The magnitude of the depression ΔT_g, of T_g for the stacked thin films from that for the bulk samples was larger than that for single thin films supported on a substrate. Here, the stacked thin films consist of 10 layers of 12-18 nm thick single thin films. 2) Annealing could result in a decrease of ΔT_g for the stacked thin films.

4.1 Thermal properties determined by differential scanning calorimetry

In this section we will show the results on the DSC measurements for the stacked PS thin films. Figure 5 shows the temperature dependence of the total heat flow during the heating process at a rate of 10 K/min for stacked PS thin films with various single layer thicknesses, as listed in Table 1. Figure 5(a) shows an anomaly in the total heat flow around 350-380 K, which is associated with the glass transition of PS, and the temperature at which the anomaly occurs can be regarded as T_g. Values of T_g, evaluated as the middle temperature of the anomalous region, are listed in Table 1. The T_g for stacked PS films increases from 350 to 369 K with increasing single layer film thickness in the stacked thin films, even if the total thickness of the stacked thin polymer films is sufficiently large to nullify the dependence of T_g on the thickness. The magnitude of the T_g depression for the stacked thin films from that for the bulk is slightly larger than that for the single thin polymer film supported on a substrate [11, 20]. In contrast, the depression for the stacked thin films is smaller than that for the freely-standing thin films [65]. This result for the T_g of stacked thin films is consistent with that reported in the literature [32,33] and with that measured by capacitance measurements for stacked P2CS thin films as shown in Fig. 4.

Figure 5(b) shows the temperature dependence of the total heat flow observed after annealing at 523 K for 12 h in vacuo. The anomalous region, i.e., T_g, is located almost at the same position, regardless of the single layer thickness. The observed value of T_g is approximately 376 K, which is almost equal to that for the bulk sample. This result suggests that T_g of the stacked thin films increases and approaches the bulk T_g after annealing at 523 K in vacuo. In other words, the bulk-like glass transition dynamics could be restored after annealing at high temperature for 12 h.

Annealing at high temperature diminishes the contrast at the interface between two thin layers, which suggests the possibility that the glass transition temperature could be controlled through interfacial interaction.

4.2 Evolution of glass transition dynamics for stacked thin films

To demonstrate the effect of annealing on the glass transition dynamics of stacked P2CS thin films in more detail, *in-situ* dielectric measurements were performed during successive isothermal annealing processes at a given annealing temperature, T_A. For these measurements several stacked thin films of P2CS were prepared, as listed in Table 2. The thickness of each single layer was between 9 and 18 nm, and the number of stacked layers for each sample for the dielectric measurements was 10. The annealing temperature was ranged between 412 and 425 K.

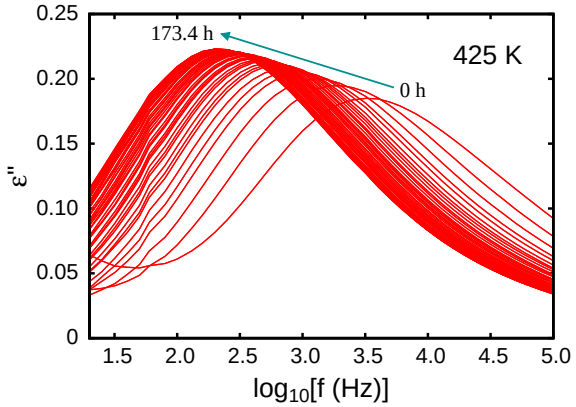

Fig. 6 Evolution of ε'' spectra as a function of annealing time t_a for the successive isothermal annealing of stacked P2CS thin films at 425 K. The thickness of each thin layer was 18 nm. The annealing times t_a were 0, 3.4, 6.8, 10, 13.4, 16.8, 20, $\cdots$, 173.4 h.

4.2.1 Shift in the dielectric loss peak due to the α-process

Figure 6 shows the evolution of the dielectric loss spectra in the frequency domain observed for the successive isothermal annealing process of stacked P2CS thin films of 18 nm thick layers. The dielectric loss ε'' vs. frequency f is plotted for various times t_a= 0$\sim$173.4 h of isothermal annealing at 425 K. The dielectric loss peak due to the α-process is located around $10^{3.6}$ Hz at t_a= 0 h. The frequency at which the dielectric loss has a peak due to the α-process is denoted by f_α. The location of the peak f_α decreases down to $10^{2.3}$ Hz and the peak height increases with increasing annealing time, which suggests a slowing of the α-process dynamics with increase in the annealing time.

As described in Sec. 2.2, two dielectric measurements in the temperature domain were conducted between two successive isothermal annealing processes for 10 h. The results suggest that there is no appreciable annealing effect of the ramping process between the repeated isothermal annealing processes for 10 h. The value of f_α for the isothermal annealing process was evaluated as a function of the annealing time t_a from the data presented in Fig. 6. Figure 7 shows the time evolution of f_α thus obtained for four different stacked thin films with various thickness and annealing temperatures.

Figure 7 shows that at the beginning of isothermal annealing, the frequencies $\log_{10} f_\alpha$ are located at 3.5, 3.3, 2.9, and 2.2 for T_A= 425, 422, 416, and 412 K, respectively. At a given T_A, the value of f_α for stacked thin films is higher than that observed for a single thin film with a thickness equal to that of a single layer in the stacked thin films. However, as the annealing time increases at a given T_A, the value of $\log_{10} f_\alpha$ decreases monotonically down to 2.4, 1.9, 1.4, and 0.75 for T_A= 425, 422, 416, and 412 K, respectively. The final values almost correspond to those observed for single thin films with thicknesses almost equivalent to the total

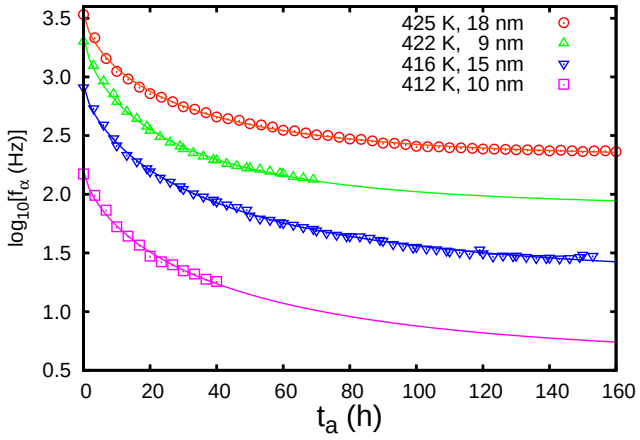

Fig. 7 Dependence of f_α on the annealing time t_a for successive isothermal annealing process at T_A= 425, 421, 416, and 412 K for stacked P2CS thin films, where the thickness of a single layer was 9-18 nm. The solid curves were calculated using Eq. (4).

Table 3 Values of f_α^∞, f_α^0, τ obtained by fitting the observed data using Eq. (4) for various annealing temperatures T_A, and the thickness of a single layer, d. Here, the exponent n is fixed at 0.70.

T_A (K)	d (nm)	$\log_{10} f_\alpha^\infty$	$\log_{10}(f_\alpha^0/f_\alpha^\infty)$	τ (h)
425	18.5	2.31 ± 0.01	1.22 ± 0.01	28.9 ± 0.7
422	9.6	1.90 ± 0.03	1.45 ± 0.02	28.0 ± 1.7
416	15.4	1.29 ± 0.01	1.65 ± 0.01	43.0 ± 1.2
412	10.0	0.6 ± 0.18	1.60 ± 0.17	45 ± 11

thickness of the stacked thin films. (See the solid curve for single thin films with the thickness of 120 nm in Fig. 13.) This result suggests that the α-dynamics of the stacked thin films approach those of thicker films with thicknesses larger than 100 nm from those of a single ultrathin film.

Figure 8 shows the dependence of T_g on the annealing time. The T_g values were determined in the temperature domain for the ramping process from measurements obtained between two successive isothermal annealing processes at T_A= 425 K for stacked thin films of 18 nm thick P2CS layers. The value of T_g was determined in the same manner described in Sec. 3. Figure 8 shows that the T_g of the stacked thin films increases with increase in the annealing time. When taking the value of T_g for the heating process in Fig. 8, then at t_a=0 the T_g of the stacked thin films is much smaller than that for a single thin film with similar thickness (T_g= 380.8 K for d= 18 nm [60]), while T_g at t_a=180 h is almost equivalent to that for the bulk (T_g= 387.8 K for d= 180 nm [60]). Although there is a slight difference in T_g between the heating and cooling processes, as usually observed in other T_g measurements,

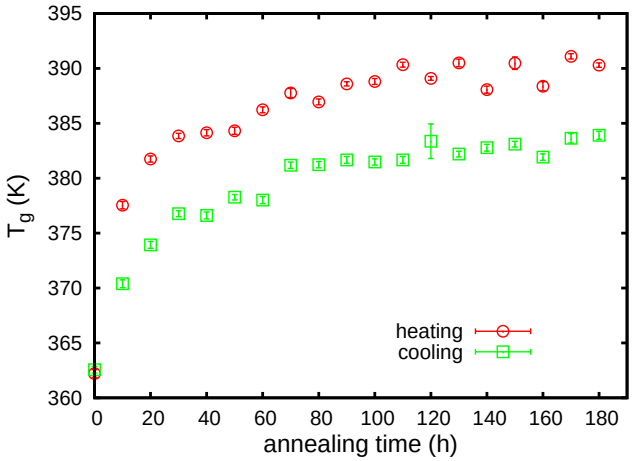

Fig. 8 Dependence of T_g on the annealing time t_a observed for the ramping process in the temperature domain between two successive isothermal annealing processes for stacked thin films of 18 nm thick P2CS layers.

the dependence of f_α on the annealing time for isothermal annealing is qualitatively consistent with the change in T_g.

The time evolution of f_α and T_g in Figs. 7 and 8 suggests that there should be a change in the dynamics of the stacked thin films with a characteristic time scale of several tens of hours for isothermal annealing.

4.2.2 Time evolution of f_α

A slow change in f_α and T_g was observed during isothermal annealing of the stacked P2CS thin films. Here, we will investigate the dependence of $f_\alpha(t_a)$ on the annealing temperature and possibly on the thickness of the single layers of the stacked thin films. Figure 7 shows that the annealing time dependence of f_α observed during the isothermal annealing process can well be reproduced using the following equation:

$$\log_{10} f_\alpha(t_a) = \log_{10} f_\alpha^\infty + (\log_{10} f_\alpha^0 - \log_{10} f_\alpha^\infty) \exp(-(t_a/\tau)^n), \tag{4}$$

where f_α^0 and f_α^∞ are the values of f_α at $t_a = 0$ and ∞, τ is the characteristic time, and n is the exponent of the stretched exponential function. The solid curves given in Fig. 7 are calculated using Eq. (4). The best fitting parameters are given in Table 3.

According to Eq. (4), the following scaling function can be obtained:

$$F_\alpha(\tilde{t}_a) = \exp(-\tilde{t}_a^n), \tag{5}$$

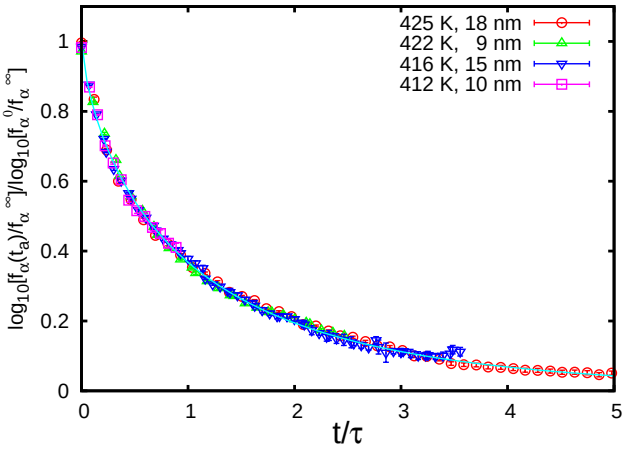

Fig. 9 $F_\alpha(\tilde{t_\alpha})$ vs. $\tilde{t}_a$ for stacked P2CS thin films for various values of T_A and d. The solid curve is calculated using Eq. (5) with n= 0.70±0.03.

where

$$F_\alpha(\tilde{t}_a) \equiv \log_{10}\left(\frac{f_\alpha}{f_\alpha^\infty}\right) / \log_{10}\left(\frac{f_\alpha^0}{f_\alpha^\infty}\right), \tag{6}$$

$$\tilde{t_a} \equiv \frac{t_a}{\tau}. \tag{7}$$

In Fig. 9, all $f_\alpha(t_a)$ data are plotted after scaling via $F_\alpha(\tilde{t}_a)$ using Eqs. (6) and (7). Figure 9 shows that the time evolution of the α-peak frequency f_α, can well be reduced to a single master curve for various values of T_A (and d). Therefore, we can expect that the observed time dependence of f_α can be controlled by a common mechanism, regardless of T_A and d. Furthermore, the exponent of Eq. (5) is given by the following relation: n=0.70±0.03. Therefore, a single exponential function could be a good approximation for this slow changing process.

Figure 10 shows the characteristic time τ for the change in the α-peak frequency f_α for this process observed during isothermal annealing at T_A. The characteristic time τ increases with decreasing annealing temperature. It should be noted that there is an ambiguity in determining the temperature dependence of τ, due to the small number of observed points. Nevertheless, if we assume that the temperature dependence of τ is given by $\tau(T_A) = \tau_0 \exp(U/T_A)$ (where τ_0 and U are the constants), then a straight line can be obtained in Fig. 10 with the parameter U = 6.2±1.9 kcal/mol. This activation energy is much smaller than of the common value for the β-process of polystyrene ($U \sim 35$ kcal/mol) [66].

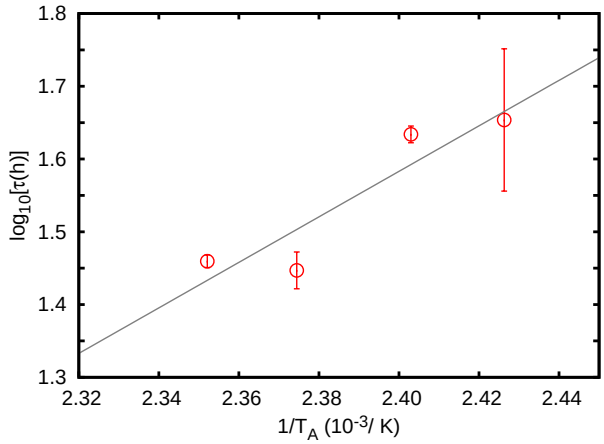

Fig. 10 Arrhenius plot of τ as a function of T_A for stacked P2CS thin films with various values of T_A and single layer thicknesses, d (9.6∼18.5 nm).

4.2.3 Diffusion of polymer chains

A change in the contrast at the interface between two neighboring layers is expected to occur during the isothermal annealing process. With increasing annealing time, the contrast decreases and, as a result, the morphology of the stacked thin film approaches that of the bulk film. It is clear that the diffusion of polymer chains is promoted during isothermal annealing, and the polymer chain undergoes interdiffusion between neighboring layers [67]. However, there is a question here as to whether the presently observed change is due solely to chain diffusion.

In order to answer this question, we estimate the chain diffusion during isothermal annealing. The temperature dependence of the diffusion constants measured using secondary ion mass spectroscopy was reported for PS by Whitlow and Wool [67]. From these measurements, we have estimated the diffusion length of P2CS for isothermal annealing at T_A, as shown in Table 4. The glass transition temperature for the bulk is T_g=388.5 K for P2CS [60] and T_g=370.5 K for PS [20], so that the difference of T_g is ΔT_g=18.0 K. Therefore, the temperature dependence of the self diffusion constant of P2CS, $D_{\mathrm{P2CS}}(T)$, was evaluated from that of PS, $D_{\mathrm{PS}}(T)$, reported in Ref. [67] using the relation $D_{\mathrm{P2CS}}(T) = D_{\mathrm{PS}}(T - 18.0\ \mathrm{K})$. The

Table 4 Diffusion constant D_{P2CS}, and diffusion length ℓ_{diff}, at two annealing temperatures for stacked P2CS thin films. D_{P2CS} is evaluated from that of PS reported in [67]. ℓ_{diff} is the diffusion length for isothermal annealing at T_A for 10 h.

T_A (K)	D_{P2CS} (cm^2/s)	ℓ_{diff} (nm)
425	9.0×10^{-16}	57
412	1.4×10^{-16}	22

values D_{P2CS} for isothermal annealing at T_A= 425 and 412 K are given in Table 4. From D_{P2CS}, the diffusion length ℓ_{diff} was also evaluated for 10 h annealing at T_A. Table 4 shows the diffusion length of P2CS is 57 nm for annealing at 425 K for 10 h. This length is much larger than the thickness of a single thin layer (d= 18 nm), even for isothermal annealing for 10 h. Therefore, it is expected that the polymer chains have already reached from one interface to the neighboring one, while the evolution of T_g and f_α still continues. However, this may be an unrealistic situation.

In order to avoid this contradictory situation, there could be two possible scenarios. Firstly, in the above discussion, we adopted the diffusion constant from Ref. [67], which was evaluated from the diffusion constant of polymer chains at the interface between two bulk polymeric layers. Recent measurements have revealed the existence of heterogeneous dynamics in confined geometries, such as thin films and nanopores [68, 69]. For stacked thin films of polymers, the dynamics vary with an essential dependence on the distance of the layer of interest from the free surface or from the substrate [70]. If such dynamical heterogeneity is taken into account, the diffusion of polymer chains could be restricted by the existence of an immobile region .

Secondly, the interface between the two polymer layers of as-stacked thin films may not be sufficiently smooth for good contact between the two layers. In this case, the diffusion of polymer chains between the two thin layers would be limited by improvement of the contact between the surfaces of the two thin layers. It has been reported that the area of indentation increases approximately with the logarithm of time for the contact of two solid surfaces. This observation is related to the change in the quality of a contact [71, 72]. As a result, the change in the interface between two thin layers could exhibit a very slow temporal change, as shown in the present measurements.

4.3 Dynamics of the α-process for stacked P2CS thin films

In this section, the time evolution of dielectric loss spectra for isothermal annealing process as a function of annealing time t_a is discussed to elucidate how the dynamics of the α-process change with increase of the annealing time t_a.

4.3.1 Shape of the dielectric spectra

Figure 11 shows the frequency dependence of the dielectric loss normalized with respect to the peak position and height of the α-process for 4 different annealing times during the isothermal annealing at T_A= 425 K for stacked thin films of 18 nm thick P2CS layers. The dielectric loss data in the frequency domain at various temperatures and at a given annealing time t_a=10$\times n$ (n is a positive integer) are extracted from the data measured for the heating process (1) between the $(n-1)$-th and n-th isothermal annealing processes (See the details in Sec. 2.2). The normalized data

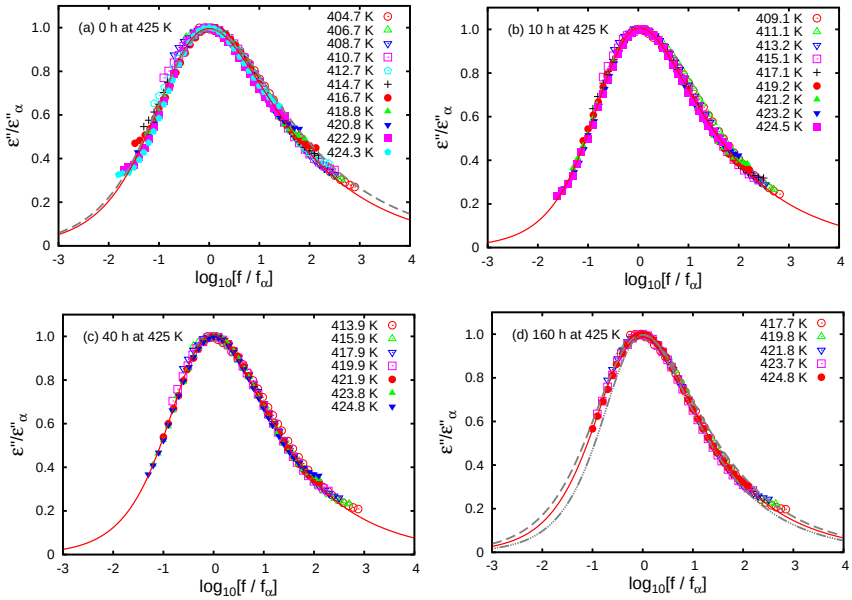

Fig. 11 Time evolution of dielectric loss spectra normalized with respect to the position of the α-process for isothermal annealing of stacked 18 nm thick P2CS thin films at T_A=425 K. The annealing times are (a) 0, (b) 10, (c) 40, and (d) 160 h. The solid curves were obtained by fitting the normalized data for the stacked thin films to Eq.(8). The dashed curves in (a) and (d) were calculated from the fitting parameters for single thin films of P2CS with thicknesses of 20 and 120 nm, respectively. The dot-dashed curve in (d) is that for stacked thin films with a thickness of 1680 nm.

shows that the superposition with respect to the position of the α-process does correspond well for the temperature range from 405 to 425 K, so that a master curve can be obtained.

As shown in Fig. 11, a master curve for the dielectric loss spectra becomes narrower with increasing annealing time for the isothermal annealing process. For comparison, the dielectric loss spectra of single thin P2CS films with thicknesses of 20, 120, and 1680 nm are given by dashed or dot-dashed curves in Figs. 11(a) and (d). This tendency in the stacked thin films is quite similar to that observed for the single thin P2CS films with increasing film thickness. Here, it should be noted that there is a slight deviation from the master curve at t_a= 0 h. The slight deviation is consistent with the existence of heterogeneity in the thin film geometry [21, 73].

Furthermore, in order to observe this narrowing of the dielectric spectra more quantitatively, the dielectric spectra were fitted in terms of the Havriliak-Negami equation:

$$\varepsilon^*(f) = \frac{\Delta\varepsilon}{(1+(i2\pi f\tau_{HN})^{1-\alpha_{HN}})^{\beta_{HN}}}, \tag{8}$$

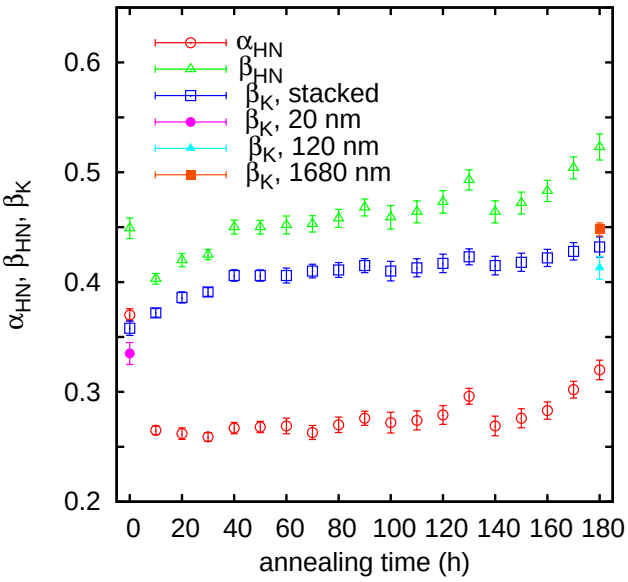

Fig. 12 Annealing time dependence of the shape parameters, α_{HN} and β_{HN}, from the HN equation, and the stretching exponent of the KWW equation β_K, for isothermal annealing at 425 K. The values of β_K are evaluated using Eq.(9). The corresponding values for single P2CS thin films with thicknesses of 20 (plotted at t_a=0), 120, and 1680 nm (plotted at t_a=180 h) are also presented for comparison.

where τ_{HN} is the relaxation time, $\Delta\varepsilon$ is the relaxation strength, and α_{HN} and β_{HN} are the shape parameters [74]. As shown by the solid curves in Fig. 11, Eq. (8) reproduces the observed master curves well at all annealing times.

Figure 12 shows the shape parameters, α_{HN} and β_{HN}, of Eq. (8) as a function of annealing time for stacked thin films of 18 nm thick P2CS layers. Both parameters increase with increasing annealing time for isothermal annealing at 425 K. Furthermore, using the α_{HN} and β_{HN} fitting parameters, the stretching parameter β_K of the Kohlrausch-Williams-Watts equation (KWW) can also be evaluated as a measure of the broadening of the relaxation time distribution [5]. See the relaxation function given by Eq. (2), where $\phi(t)$ is the relaxation function of the fluctuational correlation of dipole moments in the case of dielectric relaxation. There is an empirical relation among the α_{HN}, β_{HN}, and β_K parameters, as follows [75]:

$$\beta_K = ((1-\alpha_{HN})\beta_{HN})^{1/1.23}. \tag{9}$$

Using Eq. (9), the β_K stretching parameters can be evaluated and are found to increase with increase in the annealing time, as shown by the open square symbols in Fig. 12. In other words, the shape of the dielectric loss spectra becomes sharper with increase in the isothermal annealing time.

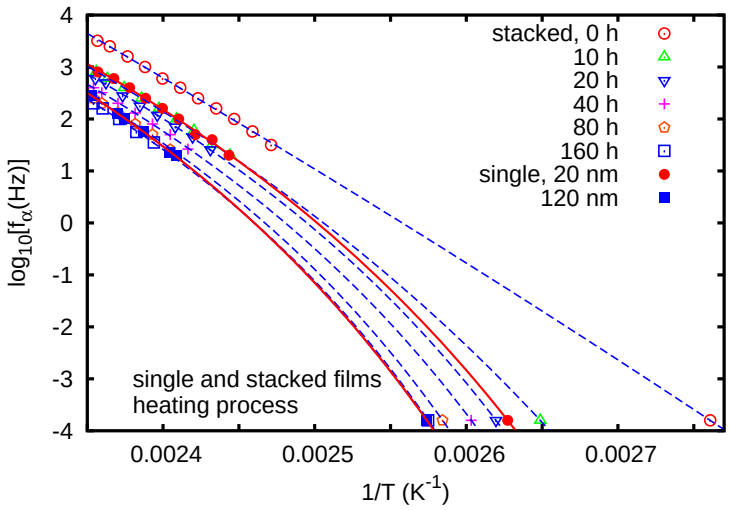

Fig. 13 Dispersion map for the α-process of both single thin films and stacked thin films of P2CS. For stacked thin films of 18 nm thick P2CS layers, the temperature dependence of f_α at various annealing times t_a=0 to 160 h are plotted. The results for single thin films with thicknesses of 20 and 120 nm are also plotted.

4.3.2 Non-Arrhenius behavior of the α-process

In order to interpret the present results both on T_g and f_α, a dispersion map of the α-process was constructed for stacked thin films of 18 nm thick P2CS layers. Figure 13 shows the data observed for single thin P2CS films with thicknesses of 20 and 120 nm together with the results for stacked thin films. Here, the values of f_α are plotted for the temperature range of 400-425 K. Furthermore, the value of T_g for a given annealing time is also plotted as the point $(1/T_g, 1/2\pi\tau_g)$, where the characteristic time of the α-process at T_g, τ_g, is assumed to be 10^3 s.

Comparison of the temperature and annealing time dependence of the relaxation times for the α-process of stacked thin films of P2CS with those for single thin films of P2CS shows that the relaxation rate of the α-process, f_α, becomes smaller with increasing annealing time for the stacked thin films, and the relaxation rate for the stacked thin films at t_a=0 is larger than that for a single thin film with a thickness of 20 nm, and f_α approaches that for the single thin film with a thickness of 120 nm with increasing annealing time. It is also noticed that for as-stacked thin films, the temperature dependence of the relaxation rate for the α-process can be well described by an Arrhenius type temperature dependence, while non-Arrhenius behavior becomes more pronounced with increasing annealing times. The curves in Fig. 13 are given by Eq. (1), where $f_\alpha = 1/2\pi\tau_\alpha$. Figure 13 shows that Eq. (1) can reproduce the observed temperature dependence of the relaxation rate of the α-process well for the isothermal annealing process. The Vogel temperature T_0 in-

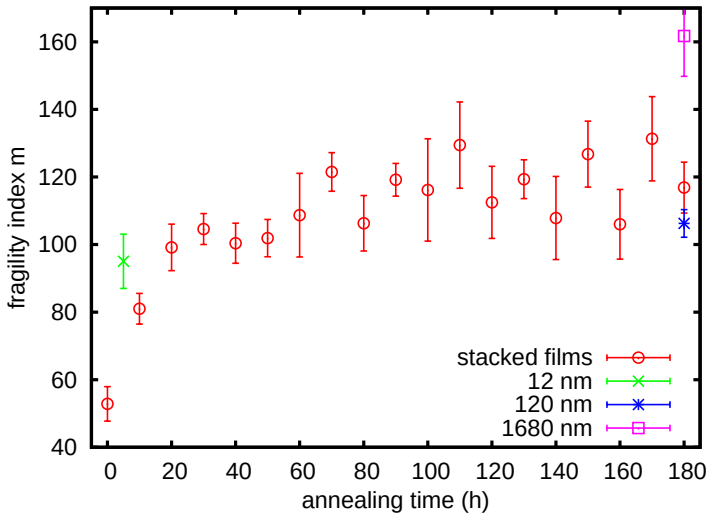

Fig. 14 Dependence of the fragility index m on the annealing time for annealing at 425 K of stacked thin films of 18 nm thick P2CS layers. The fragility indices for single thin films with thicknesses of 20, 120, and 1680 nm are also plotted.

creases with increasing annealing time, in accordance with the increase in T_g for the isothermal annealing process of stacked thin films [60,61].

In order to evaluate the non-Arrhenius behavior in more detail, the fragility index m is evaluated according to the following equation for the temperature dependence of the α-relaxation times [76]:

$$m = \left[\frac{d \log_{10} \tau_\alpha(T)}{d(T/T_g)} \right]_{T=T_g}. \tag{10}$$

Figure 14 shows that the fragility index m increases with increase in the annealing time at $T_A = 425$ K. The glassy dynamics of the stacked thin films change from less fragile to more fragile for the isothermal annealing process. The interlayer interaction within the stacked thin films of P2CS may influence the fragility of polymeric systems, because the contrast at the interface is decreased with increasing annealing time.

On the base of the present measurements, we can say that both m and β_K increase with increasing annealing time for stacked thin films of P2CS. There should be a positive correlation between m and β_K, which is totally different from that observed for conventional glassy systems that have been reported in Ref. [77,78]. However, a similar positive relationship between m and β_K was reported for the thin film geometry of PS [54]. The origin of the dynamical heterogeneity has two parts: one is an intrinsic heterogeneity related to the α-process, even in the bulk, and the other is heterogeneity induced by the geometrical restriction in thin films. The value of

β_K is determined by both factors in the case of thin polymer films, and accordingly, this leads to a different relationship between β_K and m.

Recently, the fragility index of freely standing PS films has been observed by dielectric relaxation spectroscopy and was found to decrease with decreasing film thickness down to the monomer limit [79]. The decrease in fragility index was attributed to an increase in the fraction of free surfaces in freely standing films. Comparing the present result with that of freely standing films, it should be noted that the increase in the fragility index for isothermal annealing of stacked thin polymer films might correspond to the increase in fragility index for the increase in film thickness in freely standing films. Therefore, the interface between stacked layers can play a crucial role similar to the free surface of freely standing films as long as the non-Arrhenius temperature dependence of the α-relaxation time, i.e., fragility index is concerned.

4.4 Remarks on glass transition dynamics of stacked thin films

The glass transition behavior of stacked layers of thin films of PS and P2CS was investigated using differential scanning calorimetry and dielectric relaxation spectroscopy. The results obtained can be summarized as follows:

1. Stacked thin films exhibit glass transition dynamics that are similar to those observed for single thin films. The glass transition temperature of as-stacked thin films is lower than that of the single thin supported films with the same thickness as that of a single layer in the stacked thin films, and is higher than that of freely-standing films.
2. Isothermal annealing can change the glass transition temperature and the dynamics of stacked thin films from thin film-like dynamics to bulk-like dynamics.
3. The characteristic time for evolution of the α-dynamics for stacked thin films is very large compared with the reptation time of polymer chains.
4. The relation between non-exponentiality and fragility for stacked thin films is different from that of conventional glassy systems.

In Sec. 4.2, the shift in the peak frequency of the dielectric loss due to the α-process was discussed. However, in Fig. 6, an increase in the relaxation strength, i.e., the area below the α-relaxation peak can also be observed with increase in the annealing time. The peak height in ε'' increases by 19.5 % when the annealing time elapsed from 0 h to 173.4 h. The value of ε'' plotted in Fig. 6 was not corrected for any variation in film thickness due to isothermal annealing. The variation in film thickness was found to contribute to the apparent increase in ε'' by 6.3 % from the analysis of the real part of electric capacitance at 273 K and 100 kHz for both t_a=0 h and 173.4 h. Therefore, there should be an intrinsic increase in ε'' during the isothermal annealing process. In Ref. [80], it has been reported that the relaxation strength of the α-process of the ultrathin films is smaller than that of the bulk. A possible origin of this increase in ε'' observed for the annealing of the stacked thin

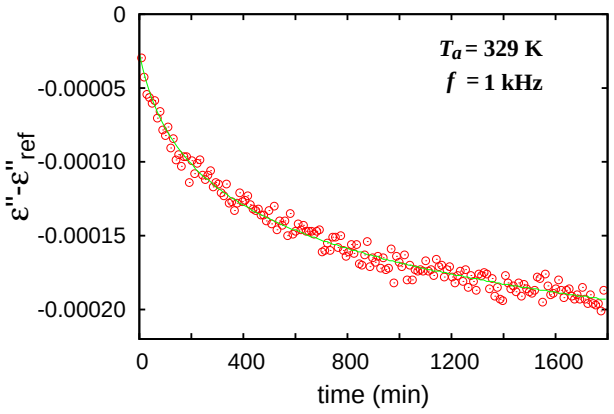

Fig. 15 Aging time dependence of $\varepsilon'' - \varepsilon''_{\rm ref}$ for P2CS thin films with d=22 nm, f=1 kHz and T_a=329 K. The solid line is fitted using Eq. (11), where $\Delta\varepsilon$=0.0082, t_0=62 min, and n=0.07.

films may be associated with the reduction of the relaxation strength of the single ultrathin polymer films. The detailed investigation of variation of the dielectric relaxation strength for P2CS and PS is now still in progress in order to elucidate the origin of the increase with annealing time.

It was discussed in Sec. 4.2 that there is a very slow change in the α-dynamics in stacked thin films of P2CS. There may be several possibilities for this slow change. If heterogeneous diffusion in thin polymer layers is an essential process, then direct measurement of diffusion constant of a tracer polymer chain in a thin layer of the stacked thin film is required. Recently, an alternative measurement of the diffusion constant of a polymer chain has been proposed [69]. Such measurements could be applicable for the present case.

If the change in the quality of the contact surface is associated with the observed phenomena, similar measurements performed under external stress are required to elucidate the strong stress dependence of the time evolution of the α-dynamics observed in stacked thin films.

Although there are many issues to be clarified, the present measurements provide clear evidence that a change in interfacial interaction is directly associated with the change in the glass transition dynamics for isothermal annealing processes.

5 Aging dynamics in ultrathin P2CS films

In the previous section, we have shown the experimental results on the glass transition dynamics above T_g, and here we move to the aging dynamics below T_g. In this section, we will discuss the second main topics, *i.e.*, the aging dynamics of the ultrathin films of P2CS. The aging time dependence of the dielectric loss ε'' relative

to the value $\varepsilon''_{\rm ref}$ is shown, as an example, in Fig. 15 for P2CS thin films undergoing isothermal aging at T_a=329 K, where $\Delta T_a \equiv T_g - T_a$= 52.9 K. The value of $\varepsilon''_{\rm ref}$ is ε'' at $t_w = 0$. This figure shows that ε'' decreases with increasing aging time, which is consistent with the results observed for PMMA thin films [38, 40]. The system approaches an equilibrium state during isothermal aging, even in the glassy state, so that the dielectric constant changes slowly with aging time. The aging time t_w dependence of ε'' can be fitted to the equation

$$\varepsilon''(t_w; f, T_a) = \frac{\Delta\varepsilon}{\left(1 + \frac{t_w}{t_0}\right)^n} + \varepsilon''(\infty; f, T_a), \tag{11}$$

where $\Delta\varepsilon$ is the relaxation strength towards the equilibrium value, t_0 is the characteristic time of the aging dynamics and n is an exponent [40]. This relation can be applied to relatively thick films. The t_w dependence for thinner films is different from this one and is discussed later.

Figure 16 shows the t_w dependence of ε'' for P2CS thin films of d=22 nm, 9.0 nm and 3.7 nm and for two different aging temperatures T_a of 348 and 310 K. The frequency of the applied electric field was 200 Hz. In Fig. 16(a), the value of ε'' decreases with increasing aging time at T_a=348 K, except for the initial stage of thin films with d=3.7 nm. However, the value of ε'' clearly *increases* for isothermal aging at T_a=310 K in the P2CS thin films with d=3.7 nm and 9.0 nm. These results suggest that the t_w dependence of ε'' is strongly dependent on the thickness and aging temperature. For thin films with d=3.7 nm, ε'' *monotonically increases* with increasing aging time at a lower aging temperature T_a(=310 K), while ε'' shows a maximum against the aging time for T_a=348 K. The latter result suggests that *there are two competing physical origins with different time scales.* Figure 16(c) shows how the aging time dependence of $\varepsilon'' - \varepsilon''_{\rm ref}$ at isothermal aging at T_a=348 K for d=3.7 nm can be decomposed into two competing, increasing and decreasing, components. Results of the detailed analyses are shown in Sec. 5.2.

Figure 17 shows the temperature dependence of the imaginary part of the dielectric constant ε'' relative to the reference value $\varepsilon''_{\rm ref}$ for the cooling process including isothermal aging for 30 h, which is observed for the constant rate mode denoted by the protocol $\mathscr{C}(T_a, t_a = 30\ h)$. Here, the values of $\varepsilon''_{\rm ref}(f, T)$ have been measured during the heating and cooling processes at a rate of 1 K/min without any isothermal aging, i.e., the protocol $\mathscr{C}(T_a, 0)$. For each temperature, the deviation $\varepsilon''(f, T) - \varepsilon''_{\rm ref}(f, T)$ was evaluated. Figure 17 shows that ε'' increases with increasing aging time t_w for isothermal aging at various aging temperature T_a, which corresponds to the increase in ε'' observed in Fig. 16. The deviation of ε'' from $\varepsilon''_{\rm ref}$ induced during the isothermal aging decreases with decreasing temperature for the subsequent cooling and ε'' approaches $\varepsilon''_{\rm ref}$. This temperature dependence shows that there is a *rejuvenation effect*, as reported for the glassy state in PMMA [38,40]. Figure 17 shows that the amount of increase in ε'' induced during isothermal aging for 30 h is not a monotonic function of the aging temperature T_a, but has a maximum at T_a=320 K. The aging temperature dependence of the amount of deviation for ultrathin P2CS films is completely different from that for PMMA [38, 40], and also for

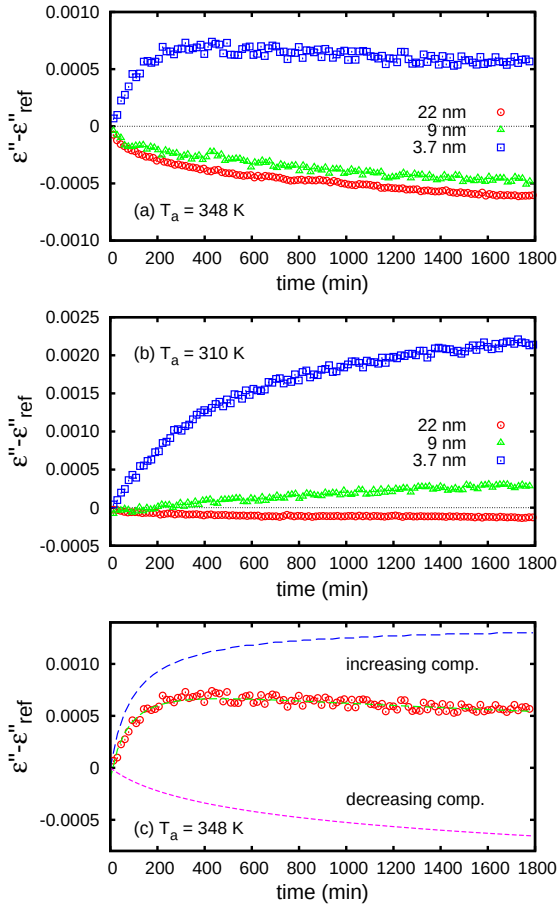

Fig. 16 Aging time dependence of $\varepsilon'' - \varepsilon''_{\rm ref}$ for P2CS thin films with d=22 nm, 9.0 nm and 3.7 nm, f=200 Hz. (a) T_a=348 K. (b) T_a=310 K. (c), aging time dependence of $\varepsilon'' - \varepsilon''_{\rm ref}$ for thin films with d=3.7 nm and f = 200 Hz, in addition to both the increasing component ($\Delta\varepsilon''_{\rm in}$, dashed line) and decreasing component ($\Delta\varepsilon''_{\rm dec}$, dotted line).

thicker films of P2CS [53]. If there is only one dynamical mode associated with the aging phenomena, then the amount of deviation should be a monotonic function of the annealing temperature. Therefore, this annealing temperature dependence also suggests that there are *two competing processes* that have different temperature dependence.

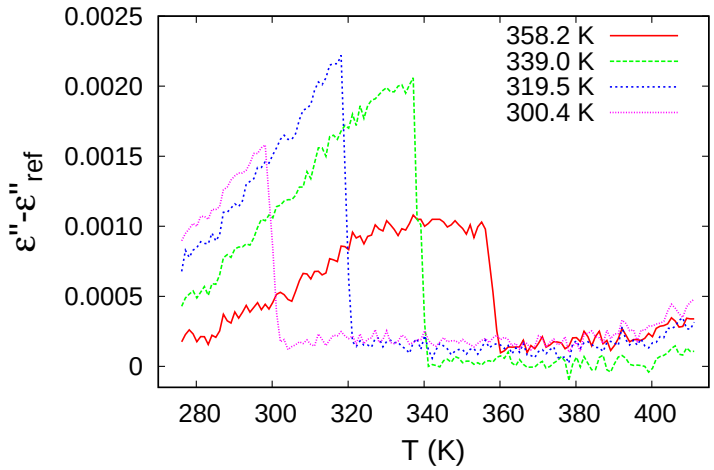

Fig. 17 Temperature dependence of the ε'' deviation from the reference values for P2CS thin films with d=3.7 nm observed during cooling, including isothermal aging at various T_a.

5.1 Segmental dynamics in ultrathin P2CS films

As discussed in the above, the aging dynamics of ultrathin P2CS films are quite different from those of thicker films, and have an anomalous dependence on the thickness and temperature. Here, the microscopic origin for such an anomaly is discussed on the basis of segmental dynamics measurements using dielectric relaxation spectroscopy.

In previous studies on PS thin films, the glass transition temperature T_g decreased with decreasing film thickness and the amount of decrease in T_g was approximately 20 K when the film thickness was decreased from the bulk value to 10 nm [11]. Accordingly, the dynamics of the α-process become faster in thinner films [20]. There are several physical reasons for the decrease in T_g and the increase in the relaxation rate of the α-process. One is the existence of a liquid-like layer with higher mobility near the free surface [31, 81]. Furthermore, the distribution of T_g within thin films is also important for the overall dynamics in thin polymer films [24, 82, 83].

Figure 18 shows the temperature dependence of ε'' for the P2CS thin films with d=9.5, 5.4, and 3.7 nm at 200 Hz. There is a loss peak due to the α-process around 415 K and the peak height decreases with decreasing film thickness. In addition to this behavior, another process around 320 K is evident only for the d=3.7 nm thin film. This peak of ε'' due to another process is also observed for thin films of both PS and PS labeled with a dye (DR1; disperse red one) [21, 73]. This extra loss peak was attributed to the segmental motion of a liquid-like layer near the surface or interface, which we have labeled as the α_l-process. The loss peak observed for ultrathin P2CS films may also be attributed to the α_l-process. If the thickness of the

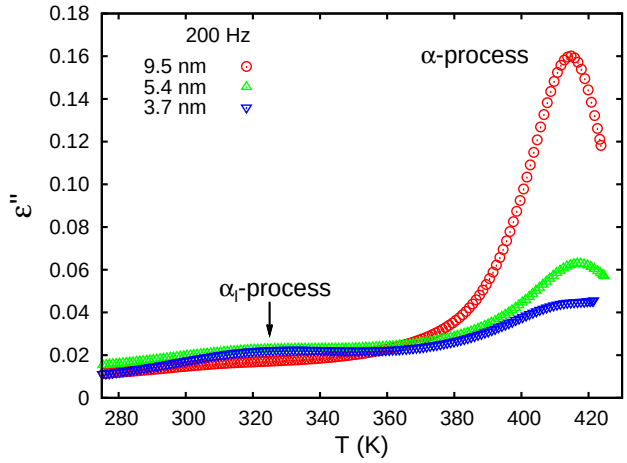

Fig. 18 Temperature dependence of the imaginary part of the complex dielectric constant ε'' for d=9.5 (○), 5.4 (△) and 3.7 nm (▽). The data points in this figure were obtained for the cooling process at f=200 Hz.

liquid-like layer is independent of the overall thickness, then the contribution of the liquid-like layer becomes more appreciable as the thickness decreases. Figure 18 shows that the dielectric loss peak due to the α-process is reduced, and accordingly, that of the α_l-process becomes more appreciable as the film thickness is decreased to d=3.7 nm.

Figure 19 shows the temperature dependence of ε'' for d=5.4 nm obtained at three different frequencies of f=20 Hz, 200 Hz, and 2 kHz. The peak due to the α_l-process is shifted to the higher temperature side as f is changed to higher frequency, which suggests that the loss peak around 300 K, the α_l-process, has dynamical character. In order to analyze the observed dielectric loss, it is assumed that there are three contributions, such as the α-process, α_l-process, and conductivity components. Therefore, we describe the complex dielectric constant ε^* as follows:

$$\varepsilon^*(f,T) = \sum_{i=\alpha,\alpha_l} \frac{\Delta\varepsilon_i}{(1+(i2\pi f\tau_i)^{1-\alpha_i})^{\beta_i}} + i\frac{\sigma}{\varepsilon_0(2\pi f)^{\gamma}}, \tag{12}$$

where the first terms on the right hand side are contributions from the α- and α_l-processes, as described by the Havriliak-Negami (HN) equations [74], $\Delta\varepsilon_i$ is the dielectric strength of the i-process, α_i and β_i are the shape parameters, and τ_i is the relaxation time. τ_i can be described by the VFT law [4],

$$\tau_i(T) = \tau_{0,i}\exp\left(\frac{T_{A,i}}{T-T_{V,i}}\right), \tag{13}$$

where $\tau_{0,i}$, $T_{A,i}$, and $T_{V,i}$ are constants. The second term on the right hand side of Eq. (12) is the contribution from the conductivity component, where γ is an ex-

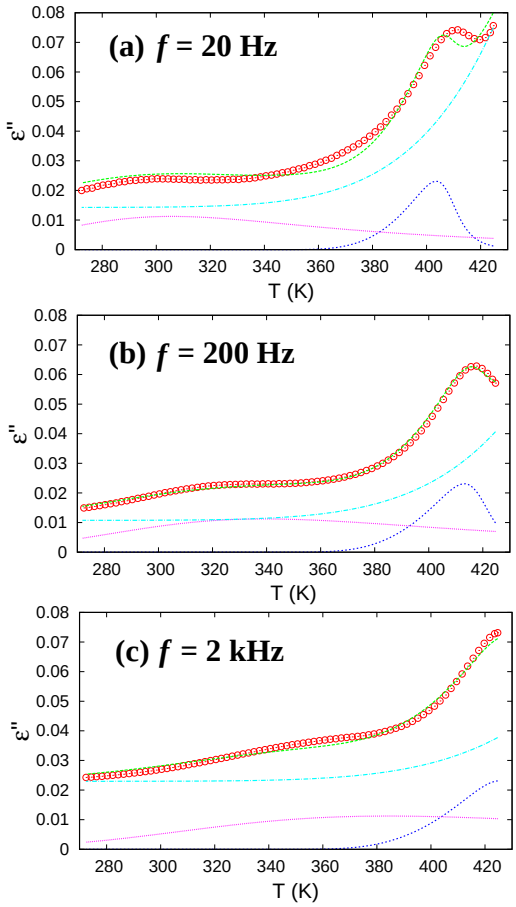

Fig. 19 (a) Temperature dependence of the imaginary part of the complex dielectric constant ε'' for P2CS thin films with d=5.4 nm obtained at f= (a) 20 Hz, (b) 200 Hz, and (c) 2 kHz. The solid line is calculated using Eq. (12) with the best-fit parameters. The dashed, dotted, and dash-dotted lines correspond to the components of the α-process, the α_l-process, and the conductivity, respectively.

ponent, ε_0 is the dielectric permittivity *in vacuo*, and σ is the conductivity. This conductivity component becomes more important as the thickness decreases. The conductivity σ can be described by using a VFT-like equation,

$$\sigma(T) = \frac{A}{T^{0.5}} \exp\left(\frac{T_{A,c}}{T - T_{V,c}}\right), \tag{14}$$

where A, $T_{A,c}$, and $T_{V,c}$ are constants [84]. The temperature dependence of ε'' can be fitted using Eq. (12) in addition to the constant background intensity. The solid curve in Fig. 19 is the curve calculated for ε'' using the best-fit parameters listed in Table 5. Each component in Eq. (12) is also shown as the dashed, dotted, and dash-dotted lines in Fig. 19. The fitting parameters listed in Table 5 are commonly obtained for the three different frequencies f=20 Hz, 200 Hz, and 2 kHz. For the

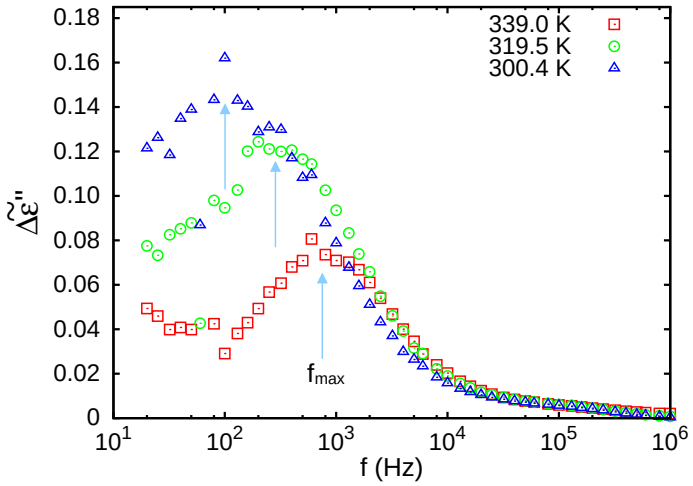

Fig. 20 Frequency dependence of $\Delta\tilde{\varepsilon}''$ after isothermal aging at three different aging temperatures T_a = 339.0 (□), 319.5 (○), and 300.4 K (△) for 30 h with d=3.7 nm.

fitting procedures, the parameters of T_{A,α_l} ($T_{A,c}$) and T_{V,α_l} ($T_{V,c}$) are assumed to be common for both the α_l-process and the conductivity component.

Table 5 Best-fit parameters for the frequency and temperature dependence of the dielectric loss ε'' observed for the P2CS ultrathin films with d=9.5, 5.4, and 3.7 nm.

process	d (nm)	1-α_i	β_i	$\tau_{0,i}$ (s)	$T_{A,i}$ (K)	$T_{V,i}$ (K)	$\Delta\varepsilon_i$
	9.5	0.68 ± 0.04	0.38 ± 0.03	$(1.8 \pm 0.2)\times10^{-12}$	1892 ± 1	324.6 ± 0.1	0.65 ± 0.03
α	5.4	0.95 ± 0.11	0.22 ± 0.04	$(5.4 \pm 1.0)\times10^{-12}$	1884.4 ± 0.9	319.6 ± 0.1	0.12 ± 0.02
	3.7	0.65 ± 0.20	0.21 ± 0.11	$(1.3 \pm 1.0)\times10^{-11}$	1750.5 ± 0.8	317.2 ± 0.1	0.075 ± 0.030
	9.5	0.26	1	3.5×10^{-8}	4.3×10^3	61	0.26±0.13
α_l	5.4	0.36 ± 0.12	1	$(1.1 \pm 4.8)\times10^{-10}$	$(4.2 \pm 2.6)\times10^3$	75 ± 92	0.078 ± 0.014
	3.7	0.42 ± 0.09	1	$(0.87 \pm 2.6)\times10^{-10}$	$(4.2 \pm 1.5)\times10^3$	72 ± 45	0.107 ± 0.010

process	d (nm)	A	γ	$T_{A,c}$	$T_{V,c}$
	9.5	2.0×10^{-5}	0.58 ± 0.24	4.3×10^3	61
conductivity comp.	5.4	7.4×10^{-6}	0.31 ± 0.04	$(4.2 \pm 2.6)\times10^3$	75 ± 92
	3.7	$(1.1 \pm 3.2)\times10^{-5}$	0.34 ± 0.04	$(4.2 \pm 1.5)\times10^3$	72 ± 45

5.2 Microscopic origin of the anomaly

Here we return to the aging dynamics that could be observed for isothermal aging at T_a. For a given frequency f, we could observe the change in $\varepsilon''(t_w; f, T_a)$ from $\varepsilon''_{\rm ref}(\equiv$

$\varepsilon''(t_w{=}0; f, T_a)$) (before isothermal aging at temperature T_a) to $\varepsilon''(t_w{=}30\ h; f, T_a)$ after isothermal aging for 30 h. Here, we define the relative relaxation strength due to the isothermal aging as

$$\Delta\tilde{\varepsilon}''(f, T_a) \equiv \frac{\varepsilon''(t_w{=}30\ h; f, T_a) - \varepsilon''(t_w{=}0; f, T_a)}{\varepsilon''(t_w{=}0; f, T_a)}. \tag{15}$$

Figure 20 shows that the relative relaxation strength $\Delta\tilde{\varepsilon}''$ has a peak against frequency, and the peak frequency $f_{\max}$ is strongly dependent on the aging temperature T_a. The frequency dependence of $\Delta\tilde{\varepsilon}''$ suggests that *there may be a relation between the aging dynamics and a dynamical mode with a characteristic time* ($\sim 1/f_{\max}$). It has been previously reported that for PMMA thin films, the relaxation strength for structural change during isothermal aging becomes larger with decreasing frequency at a given aging temperature and does not show a peak at any frequency [38, 40]. The frequency dependence of the relaxation strength due to isothermal aging for ultrathin P2CS films is completely different from that for PMMA.

A distinct peak of $\Delta\tilde{\varepsilon}''$ in the frequency domain at a given aging temperature was observed in Fig. 20. A similar behavior related to the α_l-process could also be observed in the temperature domain at a given frequency. As already shown in Fig. 16, there are two competing processes that have different aging time and temperature dependences for isothermal aging at T_a. Here, we consider the time evolution of the dielectric loss ε'' for isothermal aging at T_a. For this process, it is assumed that there are two components; $\Delta\varepsilon''_{\rm in}$ is the component that increases with aging time, and $\Delta\varepsilon''_{\rm dec}$ is the component that decreases with aging time:

$$\varepsilon''(t_w; f, T_a) - \varepsilon''_{\rm ref} = \Delta\varepsilon''_{\rm in}(t_w; f, T_a) + \Delta\varepsilon''_{\rm dec}(t_w; f, T_a), \tag{16}$$

where

$$\varepsilon''_{\rm ref} \equiv \varepsilon''(t_w{=}0; f, T_a) \tag{17}$$

$$\Delta\varepsilon''_{\rm in}(t_w; f, T_a) \equiv \Delta\varepsilon_l \left[1 - \left(1 + \frac{t_w}{t_l}\right)^{-n_l}\right] \tag{18}$$

$$\Delta\varepsilon''_{\rm dec}(t_w; f, T_a) \equiv \Delta\varepsilon_b \left[\left(1 + \frac{t_w}{t_b}\right)^{-n_b} - 1\right] \tag{19}$$

The values t_l and t_b are the characteristic times, and n_l and n_b are the exponents, and $\Delta\varepsilon_l$ and $\Delta\varepsilon_b$ are the relaxation strengths for the increasing and decreasing components, respectively. Here, we have decomposed the time evolution of $\varepsilon'' - \varepsilon''_{\rm ref}$ into two competing components, $\Delta\varepsilon''_{\rm in}$ and $\Delta\varepsilon''_{\rm dec}$, using Eqs. (18) and (19) for isothermal aging at T_a and three different frequencies for ultrathin P2CS films with d=3.7 nm. The best fit parameters for the time evolution of $\varepsilon'' - \varepsilon''_{\rm ref}$ for isothermal aging at T_a are listed in Table 6. For the fitting procedures, the parameter n_l is fixed to 1 and the parameters t_b and n_b for fitting the data for d=3.7 nm are fixed to those obtained by fitting the observed data to Eq. (19) with 2 and 4 kHz for d=22 nm. For the de-

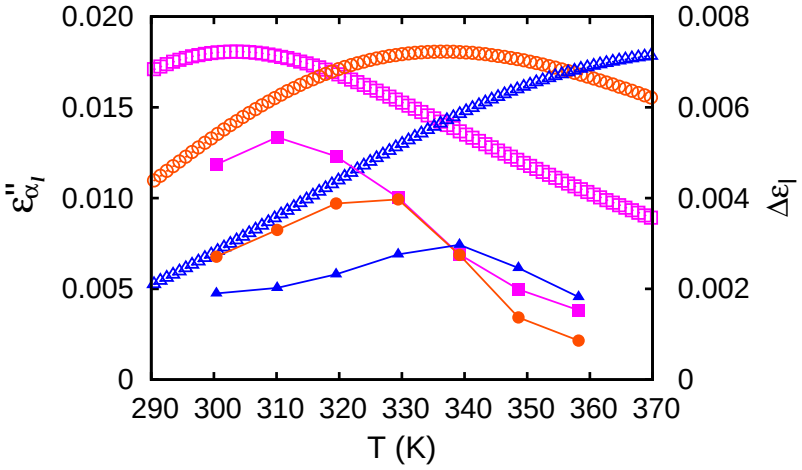

Fig. 21 Temperature dependence of the α_l-process component of dielectric loss, $\varepsilon''_{\alpha,l}$, at f=20 Hz (□), 200 Hz (○) and 2 kHz (△) and aging temperature dependence of the increasing ε'' component during isothermal aging, $\Delta\varepsilon_l$ at f=20 Hz (■), 200 Hz (●) and 2 kHz (▲).

creasing component $\Delta\varepsilon''_{\rm dec}$, only the value of $\Delta\varepsilon_b$ is adjusted in order to reproduce the observed results for d=3.7 nm at the three different frequencies. An example of the decomposition of ε'' into $\Delta\varepsilon''_{\rm in}$ and $\Delta\varepsilon''_{\rm dec}$ is shown in Fig. 16(c).

From the decomposition procedures, we have obtained the relaxation strength $\Delta\varepsilon_l$ of the increasing components as a function of the aging temperature T_a for given frequencies of f=20 Hz, 200 Hz, and 2 kHz. (See the full symbols in Fig. 21.) In order to compare the aging dynamics with the dynamical mode of the α_l-process, we also plotted in Fig. 21 the component of ε'' only for the α_l-process, ε''_{α_l}, that has been reproduced using the HN equation with the best-fit parameters for the α_l-process listed in Table 5 (See the open symbols in Fig. 21). Figure 21 shows that the temperature dependence of the aging strength due to the increasing component is strongly associated with that of the dielectric loss due only to the α_l-process.

Table 6 Best fit parameters for the aging time dependence of $\varepsilon'' - \varepsilon''_{\rm ref}$ for isothermal aging at T_a=300-358 K and for f=2 kHz, 200 Hz, and 20 Hz.

	f=2 kHz			f=200 Hz			f=20 Hz				
T_a(K)	$\Delta\varepsilon_l$	t_l (min)	$\Delta\varepsilon_b$	$\Delta\varepsilon_l$	t_l (min)	$\Delta\varepsilon_b$	$\Delta\varepsilon_l$	t_l (min)	$\Delta\varepsilon_b$	t_b (min)	n_b
358.2	0.00183	102 ± 1	0.00558	0.00085	61 ± 3	0.00349	0.00153	68 ± 2	0.00741	45 ± 1	0.036 ± 0.003
348.6	0.00247	165 ± 2	0.00603	0.00137	97 ± 3	0.00636	0.00198	122 ± 3	0.01046	157 ± 3	0.043 ± 0.005
339.2	0.00300	233 ± 2	0.00839	0.00275	178 ± 4	0.01969	0.00275	153 ± 2	0.02216	120 ± 6	0.026 ± 0.009
329.4	0.00278	324 ± 2	0.00483	0.00396	250 ± 3	0.03159	0.00402	199 ± 2	0.04524	76 ± 4	0.017 ± 0.011
319.5	0.00232	402 ± 2	0	0.00387	413 ± 9	0.02705	0.00491	391 ± 5	0.07393	317 ± 12	0.018 ± 0.009
310.1	0.00202	450 ± 2	0	0.00329	471 ± 5	0.01145	0.00533	418 ± 3	0.06581	113 ± 12	0.010 ± 0.020
300.4	0.00189	634 ± 5	0	0.00272	632 ± 6	0	0.00472	614 ± 5	0.05685	220 ± 30	0.010 ± 0.040

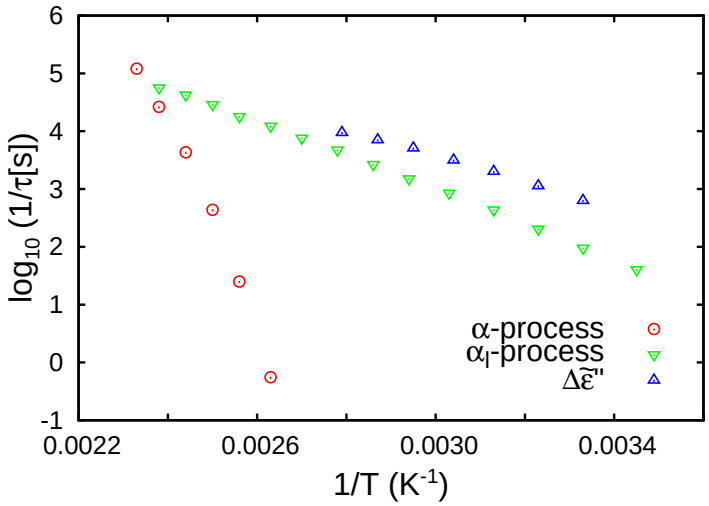

Fig. 22 Arrhenius plots for the α- and α_l-processes of ultrathin P2CS films with d=3.7 nm. The value of τ is evaluated from the relationship $1/2\pi\tau = f_{\max}, f_\alpha$, or f_{α_l}. The symbol $\circ$ corresponds to the data obtained from the peak frequency f_α of the dielectric loss ε'' due only to the α-process, which is evaluated by fitting the observed values of ε'' to Eq. (12). The symbol $\triangledown$ corresponds to the data obtained from f_{α_l} due only to the α_l-process. The symbol $\triangle$ corresponds to the peak frequency of $\Delta\tilde{\varepsilon}''$, $f_{\max}$, in Fig. 20 at a given aging temperature T_a.

Figure 22 shows Arrhenius plots of the relaxation times for the α- and α_l-processes obtained by the peak frequency of the dielectric loss ε'' for P2CS thin films with d =3.7 nm. The peak frequencies f_α and f_{α_l} are evaluated from the frequency dependence of the dielectric loss due only to the α- and α_l-processes that are reproduced from Eq. (12) with best fit parameters. The peak frequency of $\Delta\tilde{\varepsilon}''(f, T_a)$ after isothermal aging at a given aging temperature T_a for 30 h and with d=3.7 nm is also plotted in Fig. 22. The peak frequency is evaluated from the observed frequency dependence of $\Delta\tilde{\varepsilon}''$ in Fig. 20.

From Fig. 22, the temperature dependence of the characteristic time τ evaluated from the aging dynamics ($\triangle$) is quite similar to that evaluated from the dynamics of the α_l-process ($\triangledown$), but is completely different from that evaluated from the dynamics of the α-process ($\circ$). Therefore, it can be concluded that the anomalous increase in dielectric susceptibility observed for isothermal aging of ultrathin P2CS films is strongly associated with the α_l-process.

5.3 Remarks on anomaly observed in aging dynamics in ultrathin P2CS films

Occurrence of the α_l-process may lead to the increase in the dielectric susceptibility with isothermal aging of P2CS ultrathin films. The most probable candidate for the microscopic origin of the α_l-process is the presence of a mobile interfacial region where the polymer chains can maintain their mobility, even below the bulk T_g. Such mobility can destroy the "ordering" that is developed during the aging process. In other words, the mobility can rejuvenate the glassy state for ultrathin films of P2CS.

The present measurements showed that the dielectric susceptibility increases with increasing aging time for the isothermal aging of ultrathin P2CS films. Here, we have a question on how the mobile layer can increase the dielectric susceptibility with increasing aging time. For thin polymer films, de Gennes proposed that there is a sliding motion for the thin film geometry of polymers [85, 86]. Even in the glassy state, a polymer chain can move along its own contour if there is a interfacial mobile layer.

The occurrence of the sliding motion can cause polymer chains in the bulk region to move to the mobile region near the interface during isothermal aging. The number of polymer chains that belong to the mobile region increases, and the fraction of polymer chains that contribute to the α_l-process increases. This phenomenon manifests as an increase of ε'' for isothermal aging at a given temperature and frequency. We propose this as a possible scenario for the present anomalous increase in ε'' for isothermal aging.

Our previous measurements of P2CS thin films with thicknesses greater than 10 nm showed that both the dielectric susceptibility and volume decrease with increase in the aging time for isothermal aging [53]. The decrease in volume causes an increase in the electric capacitance. In this case, the decrease in dielectric susceptibility competes with the decrease in volume for determination of the aging time dependence of the electric capacitance. Therefore, we consider the possibility that the volume change during isothermal aging could cause an artificial increase in the dielectric susceptibility. Table 7 shows the decrease in volume and the increase in the imaginary part of the electric capacitance C'' for isothermal aging at T_a= 300-358 K. The increment in C'' is far greater than the decrease in volume; therefore, the possibility of an artificial increase is denied.

As a summary in Sec. 5, we have observed an anomalous increase in the dielectric susceptibility for the isothermal aging of ultrathin P2CS films below T_g, and the fraction of the interfacial mobile region where the polymer chains are mobile as observed in a liquid state can increase in accordance with the increase in dielectric susceptibility.

Table 7 Relative decrease in volume for isothermal aging at T_a for 30 h, $\Delta\tilde{v} \equiv -(v(t_w{=}30\ h) - v(t_w{=}0))/v(t_w{=}0)$, where $v(t_w)$ is the volume at time t_w, the maximum relative deviation of C'' from the initial value at t_w=0 during isothermal aging, $\Delta\tilde{C''} \equiv (C''(t_w{=}t_{\max}) - C''(t_w{=}0))/C''(t_w{=}0)$, where $C''(t_w)$ is the imaginary part of the complex electric capacitance at t_w for an applied electric field frequency of f=1 kHz, and $t_{\max}$ is the time at which C'' has a maximum during isothermal aging, and the ratio between $\Delta\tilde{C''}$ and $\Delta\tilde{v}$.

T_a (K)	$\Delta\tilde{v}$	$\Delta\tilde{C''}$	$\Delta\tilde{C''}/\Delta\tilde{v}$
300	0.114	8.44×10^{-2}	74.1
319	0.136	9.93×10^{-2}	73.0
339	0.159	7.44×10^{-2}	46.7
358	0.230	2.90×10^{-2}	12.6

6 Summary

In this article, we have discussed two different topics related to the glass transition of thin polymer films. As the first topic, we have showed the experimental results of the glass transition and α-dynamics of stacked thin polymer films measured by DSC and dielectric relaxation spectroscopy. It has been revealed that interfacial interaction can play a crucial role in determining how the glass transition temperature deviates from the value of the bulk system if the thickness decreases from the bulk one. Furthermore, the annealing above T_g can induce the change in the interfacial interaction between thin layers, and hence this can control the fragility and the non-Arrhenius behavior.

Then, as the second topic, we have discussed an anomalous phenomenon observed for the aging dynamics in single ultrathin polymer films. From this study, it has been elucidated that the anomalous increase in dielectric susceptibility observed for isothermal aging process is strongly associated with the mobile region which exists at the surface and interfacial region of thin polymer films.

The researches on the glass transition of thin polymer films have started in 1990s for the purpose of determining the existence and the nature of the characteristic length scale of the dynamics such as dynamical heterogeneity. However, as a by-product, the researches have clarified that heterogeneous dynamics strongly influence the α-process and the aging phenomena observed above and below T_g, respectively, and, as a result, produce many fascinating phenomena. Here, the heterogeneous dynamics include the mobile regions near the surface and/or interface, and heterogeneity induced by the geometrical constraint in thin films. These phenomena seem very complex, but it can be expected that they are strongly associated with each other. From the various experimental results related to the phenomena, we will be able to extract the essence of the glass transition and reach the final goal of the understanding of the mechanism of glass transition.

Acknowledgements This work was supported by a Grant-in-Aid for Scientific Research (B) (No. 21340121) and Exploratory Research (No. 23654154) from the Japan Society for the Promotion of Science, Scientific Research in the Priority Area “Soft Matter Physics” and “High-Tech

Research Center" Project for Private Universities: matching fund subsidy from the Ministry of Education, Culture, Sports, Science and Technology of Japan.

References

1. Ngai KL (2003) The glass transition and the glassy state. In: Mark J (ed) Physical Properties of Polymers, 3rd edn. Cambridge Univ Press, Cambridge
2. Anderson PW (1995) Through the glassy lightly. Science 267:1609-1618
3. Ngai KL (ed) (1991) Proceedings of the 1st-6th International Discussion Meetings on Relaxations in Complex Systems J Non-Cryst Solids 131-133; (1994) *ibid.* 172-174; (1998) *ibid.* 235-237; (2002) *ibid.* 307-310; (2006) *ibid.* 352:4371-5250; (2011) *ibid.* 357:241-782
4. Vogel H (1921) Das Temperatur-Abhängigkeitsgesetz der Viskosität von Flüssigkeiten. Phys Z 22:645-646: Fulcher GS (1925) Analysis of recent measurements of the viscosity of glasses. J Am Ceramic Soc 8:339-355: Tammann G, Hesse W (1926) Die Abhängigkeit der Viscosität von der Temperatur bei unterkühlten Flüssigkeiten. Z Anorg Allg Chem 156:245-256
5. Williams G, Watts DC (1970) Non-symmetrical dielectric relaxation behaviour arising from a simple empirical decay function. Trans Faraday Soc 66:80-85
6. Sillescu H (1999) Heterogeneity at the glass transition: a review. J Non-Cryst Solids 243:81-108
7. Berthier L, Biroli G, Bouchaud J-P, Cipelletti L, van Saarloos W (ed) (2010) Dynamical Heterogeneities in Glasses, Colloids and Granular Media, Oxford Univ Press, New York
8. Adam G, Gibbs JH (1965) On the temperature dependence of cooperative relaxation properties in glass-forming liquids. J Chem Phys, 43:139-146
9. Forrest JA, Dalnoki-Veress K, Dutcher JR (1997) Interface and chain confinement effects on the glass transition temperature of thin polymer films. Phys Rev E 56:5705-5716
10. Alcoutlabi M, McKenna GB (2005) Effects of confinement on material behavior at the nanometer size scale. J Phys: Condens Matter 17:R461-R524
11. Keddie J, Jones RAL, Cory RA (1994) Size-Dependent Depression of the Glass Transition Temperature in Polymer Films. Europhys Lett 27:59-64
12. Keddie JL, Jones RAL (1994) Interface and surface effects on the glass-transition temperature in thin polymer films. Faraday Discuss 98:219-230
13. Schüller J, Mel'nichenko YuB, Richert R, Fischer EW (1994) Dielectric studies of the glass transition in porous media. Phys Rev Lett 73:2224-2227
14. DeMaggio GB, Frieze WE, Gidley DW, Ming Zhu, Hristov HA, Yee AF (1997) Interface and surface effects on the glass transition in thin polystyrene Films. Phys Rev Lett 78:1524-1527
15. Wallace WE, van Zanten JH, Wu WL (1995) Influence of an impenetrable interface on a polymer glass-transition temperature. Phys Rev E 52:R3329-R3332
16. Jerome B, Commandeur J (1997) Dynamics of glasses below the glass transition. Nature 386:589-592
17. Efremov MYu, Olson EA, Zhang M, Zhang Z, Allen LH (2003) Glass transition in ultrathin polymer films: calorimetric study. Phys Rev Lett 91:085703
18. Lupascu V, Huth H, Schick C, Wübbenhorst M (2005) Specific heat and dielectric relaxations in ultra-thin polystyrene layers. Thermochim Acta 432:222-228
19. Hall DB, Hooker JC, Torkelson JM (1997) Ultrathin polymer films near the glass transition: effect on the distribution of alpha-relaxation times as measured by second harmonic generation. Macromolecules 30:667-669
20. Fukao K, Miyamoto Y (1999) Glass transition temperature and dynamics of α-process in thin polymer films. Europhys Lett 46:649-654
21. Fukao K, Miyamoto Y (2000) Glass transitions and dynamics in thin polymer films: Dielectric relaxation of thin films of polystyrene. Phys Rev E 61:1743-1754
22. Grohens Y, Hamon L, Reiter G, Soldera A, Holl Y (2002) Some relevant parameters affecting the glass transition of supported ultra-thin polymer films. Eur Phys J E 8:217-224

23. Sharp JS, Forrest JA (2003) Dielectric and ellipsometric studies of the dynamics in thin films of isotactic poly(methylmethacrylate) with one free surface. Phys Rev E 67:031805
24. Ellison CJ, Torkelson JM (2003) The distribution of glass-transition temperatures in nanoscopically confined glass formers. Nature Materials 2:695-700
25. Roth CB, Dutcher JR (2003) Glass transition temperature of freely-standing films of atactic poly(methyl methacrylate). Eur Phys J E 12:S103-S107
26. Ellison CJ, Mundra MK, Torkelson JM (2005) Impacts of polystyrene molecular weight and modification to the repeat unit structure on the glass transition-nanoconfinement effect and the cooperativity length scale. Macromolecules 38:1767-1778
27. Arndt M, Stannarius R, Groothues H, Hempel E, Kremer F (1997) Length scale of cooperativity in the dynamic glass transition. Phys Rev Lett 79:2077-2080
28. Hartmann L, Gorbatschow W, Hauwende J, Kremer F (2002) Molecular dynamics in thin films of isotactic poly(methyl methacrylate). Eur Phys J E 8:145-154
29. Huth H, Minakov AA, Serghei A, Kremer F, Schick C (2007) Differential ac-chip calorimeter for glass transition measurements in ultra thin polymeric films. Euro Phys J-Special Topics 141:153-160
30. Tress M, Erber M, Mapesa EU, Huth H, Mller J, Serghei A, Schick C, Eichhorn K-J, Voit B, Kremer F (2010) Glassy dynamics and glass transition in nanometric thin layers of polystyrene. Macromolecules 43:9937-9944
31. Kajiyama T, Tanaka K, Ohki I, Ge S-R, Yoon SJ, Takahara A (1994) Imaging of dynamic viscoelastic properties of a phase-separated polymer surface by forced oscillation atomic force microscopy. Macromolecules 27:7932-7934
32. Koh YP, McKenna GB, Simon SL (2006) Calorimetric glass transition temperature and absolute heat capacity of polystyrene ultrathin films. J Polym Sci, Part B: Polym Phys 44:3518-3527
33. Koh YP, Simon SL (2008) Structural relaxation of stacked ultrathin polystyrene films. J Polym Sci Part B: Polym Phys 46:2741-2753
34. Strobl G (1996) The physics of polymers: concepts for understanding their structures and behavior, Springer Verlag, Berlin
35. Struick LC (1978) Physical aging in amorphous polymers and other materials, Elsevier, Amsterdam
36. Kovacs AJ, Aklonis JJ, Hutchinson JM, Ramos AA (1979) Isobaric volume and enthalpy recovery of glasses II. a transparent multiparameter theory. J Polym Sci: Polym Phys Ed 17:1097-1162
37. Bouchaud J-P (2000) Aging in glassy systems: experiments, models, and open questions. In Cates ME, Evans MR (ed) Soft and fragile matter, IOP publishing, London 285-304
38. Bellon L, Ciliberto S, Laroche C (2002) Advanced memory effects in the aging of a polymer glass. Eur Phys J B 25:223-231
39. Bellon L, Ciliberto S, Laroche C, cond-mat/9905160
40. Fukao K, Sakamoto A (2005) Aging phenomena in poly(methyl methacrylate) thin films: Memory and rejuvenation effects. Phys Rev E 71:041803
41. Fukao K, Sakamoto A, Kubota Y, Saruyama Y (2005) Aging phenomena in poly(methyl methacrylate) by dielectric spectroscopy and temperature modulated DSC. J Non-Crysalline Solids 351:2678-2684
42. Fukao K, Yamawaki S (2007) Crossover of aging dynamics in polymer glass: From cumulative aging to noncumulative aging. Phys Rev E 76:021507
43. Bodiguel H, Lequeux F, Montes H (2008) Revealing the respective effect of aging and cyclic deformation through the memory effect in glassy polymers. J Stat Mech P01020
44. Lefloch F, Hammann J, Ocio M, Vincent E (1992) Can Aging Phenomena Discriminate Between the Droplet Model and a Hierarchical Description in Spin Glasses? Europhys Lett 18:647-652
45. Vincent E, Bouchaud J-P, Hamman J, Lefloch F (1995) Contrasting effects of field and temperature variations on ageing in spin glasses. Phil Mag B 71:489-500
46. Jonason K, Vincent E, Hammann J, Bouchaud J-P, Nordblad P (1998) Memory and chaos effects in spin glasses. Phys Rev Lett 81:3243-3246

47. Jonason K, Nordblad P, Vincent E, Hammann J, Bouchaud J-P (2000) Memory interference effects in spin glasses. Eur Phys J B 13:99-105
48. Doussineau P, de Lacerda-Aroso T, Levelut A (1999) Aging and memory effects in a disordered crystal. Europhys Lett 46:401-406
49. Leheny RL, Nagel SR (1998) Frequency-domain study of physical aging in a simple liquid. Phys Rev B 57:5154-5162
50. Kircher O, Böhmer R (2002) Probing electron-phonon coupling in high-T_c superconductors by site-selective isotope substitution. Eur Phys J B 26:329-338
51. Fukao K, Koizumi H (2007) Aging phenomena in polystyrene thin films. Eur Phys J Special Topics 141:199-202
52. Fukao K, Koizumi H (2008) Glassy dynamics in thin films of polystyrene. Phys Rev E 77:021503
53. Fukao K, Tahara D (2009) Aging dynamics in the polymer glass of poly(2-chlorostyrene): Dielectric susceptibility and volume. Phys Rev E 80:051802
54. Fukao K, Miyamoto Y (2001) Slow dynamics near glass transitions in thin polymer films. Phys Rev E 64:011803
55. Fukao K (2008) Dielectric behavior of glass transition and dynamics in thin polymer films. Nihon Reoroji Gakkaishi (J Soc Rheology Japan) 36:73-80
56. Kawana S, Jones RAL (2003) Effect of physical ageing in thin glassy polymer films. Eur Phys J E 10:223-230
57. Ellison CJ, Kim SD, Hall DB, Torkelson JM (2002) Confinement and processing effects on glass transition temperature and physical aging in ultrathin polymer films: Novel fluorescence measurements. Eur Phys J E 8:155-166
58. Priestley RD, Ellison CJ, Broadbelt LJ, Torkelson JM (2005) Structural relaxation of polymer glasses at surfaces, interfaces, and in between. Science 309:456-459
59. Priestley RD, Broadbelt LJ, Torkelson JM (2005) Physical aging of ultrathin polymer films above and below the bulk glass transition temperature: effects of attractive vs neutral polymer − substrate interactions measured by fluorescence. Macromolecules 38:654-657
60. Fukao K, Oda Y, Nakamura K, Tahara D (2010) Glass transition and dynamics of single and stacked thin films of poly(2-chlorostyrene). Euro Phys J Special Topics 189:165-171
61. Fukao K, Terasawa T, Oda Y, Nakamura K, Tahara D (2011) Glass transition dynamics of stacked thin polymer films. Phys Rev E 84:041808
62. Tahara D, Fukao K (2010) Anomalous increase in dielectric susceptibility during isothermal aging of ultrathin polymer films. Phys Rev E 82:051801
63. Tsagaropoulos G, Eisenberg A (1995) Dynamic mechanical study of the factors affecting the two glass transition behavior of filled polymers. similarities and differences with random ionomers. Macromolecules 28:6067-6077
64. Tanaka K, Tateishi Y, Okada Y, Nagamura T, Doi M, Morita H (2009) Interfacial mobility of polymers on inorganic solids. J Phys Chem B 113:4571-4577
65. Forrest JA, Dalnoki-Veress K, Stevens JR, Dutcher JR (1996) Effect of free surfaces on the glass transition temperature of thin polymer films. Phys Rev Lett 77:2002-2005
66. McCrum NG, Read BE, Williams G (1967) Anelastic and dielectric effects in polymer solids, John Wiley & Sons, London, 414, Figure 10.35
67. Whitlow SJ, Wool RP (1991) Diffusion of polymers at interfaces: a secondary ion mass spectroscopy study. Macromolecules 24:5926-5938
68. Napolitano S, Wübbenhorst M (2011) The lifetime of the deviations from bulk behaviour in polymers confined at the nanoscale. Nature Comm 2:260
69. Napolitano S, Rotella C, Wübbenhorst M (2011) Is the reduction in tracer diffusivity under nanoscopic confinement related to a frustrated segmental mobility? Macromol Rapid Comm 32:844-848
70. Inoue R, Kawashima K, Matsui K, Kanaya T, Nishida K, Matsuba G, Hino M (2011) Distributions of glass-transition temperature and thermal expansivity in multilayered polystyrene thin films studied by neutron reflectivity. Phys Rev E 83:021801
71. Bowden FB, Tabor D (1954) The friction and lubrication of solids, Clarendon, Oxford

72. Dieterich JH, Conrad G (1984) Effect of humidity on time- and velocity-dependent friction in rocks. J Geophys Res 89:4196-4202
73. Priestley RD, Broadbelt LJ, Torkelson JM, Fukao K (2007) Glass transition and α-relaxation dynamics of thin films of labeled polystyrene. Phys Rev E 75:061806
74. Havriliak S, Negami S (1967) A complex plane representation of dielectric and mechanical relaxation processes in some polymers. Polymer 8:161-210
75. Alvarez F, Alegria A, Colmenero J (1991) Relationship between the time-domain Kohlrausch-Williams-Watts and frequency-domain Havriliak-Negami relaxation functions. Phys Rev B 44:7306-7312
76. Böhmer R, Angell CA (1992) Correlations of the nonexponentiality and state dependence of mechanical relaxations with bond connectivity in Ge-As-Se supercooled liquids. Phys Rev B 45:10091-10094
77. Böhmer R, Ngai KL, Angell CA, Plazek DJ (1993) Nonexponential relaxations in strong and fragile glass formers. J Chem Phys 99:4201-4209
78. Debenedetti PG, Stillinger FH (2001) Supercooled liquids and the glass transition. Nature (London) 410:259-267
79. Napolitano S, Wübbenhorst M (2010) Structural relaxation and dynamic fragility of freely standing polymer films. Polymer 51:5309-5312
80. Fukao K, Uno S, Miyamoto Y, Hoshino A, Miyaji H (2001) Dynamics of α and β processes in thin polymer films: poly(vinyl acetate) and poly(methyl methacrylate). Phys Rev E 64:051807
81. Akabori K, Tanaka K, Nagamura T, Takahara A, Kajiyama T (2005) Molecular motion in ultrathin polystyrene films: dynamic mechanical analysis of surface and interfacial effects. Macromolecules 38:9735-9741
82. Kanaya T, Inoue R, Kawashima K, Miyazaki T, Tsukushi I, Shibata T, Matsuba G, Nishida K, Hino M (2009) Glassy dynamics and heterogeneity of polymer thin films. J Phys Soc Japan 78:041004
83. Kawashima K, Inoue R, Kanaya T, Matsuba G, Nishida K, Hino M (2009) Distribution of glass transition temperature Tg in a polymer thin film by neutron reflectivity. J Phys: Conf Ser 184:012004
84. Jeevanandam P, Vasudevan S (1998) Conductivity of a confined polymer electrolyte: Lithium-polypropylene Glycol intercalated in layered CdPS3. J Phys Chem B 102:4753-4758
85. de Gennes PG (2000) Glass transitions in thin polymer films. Eur Phys J E 2:201-205
86. de Gennes PG (2000) Glass transitions of freely suspended polymer films. C R Acd Sci IV-Phys 1:1179-1186